Defense Threat Reduction Agency
8725 John J. Kingman Road, MS-6201
Fort Belvoir, VA 22060-6201

DTRA–TR–16–059

TECHNICAL REPORT

A Mathematical Model of the Human Small Intestine Following Acute Radiation and Burn Exposures

August 2016

HDTRA1–14–D–0003; 0005

Prepared by:

Applied Research Associates, Inc.
801 N. Quincy Street
Suite 700
Arlington, VA 22203

REPORT DOCUMENTATION PAGE

Form Approved
OMB No. 0704-0188

1. REPORT DATE *(DD-MM-YYYY)*	2. REPORT TYPE	3. DATES COVERED *(From - To)*
04-08-2016	Technical Report	

4. TITLE AND SUBTITLE

A Mathematical Model of the Human Small Intestine Following Acute Radiation and Burn Exposures

5a. CONTRACT NUMBER

HDTRA1-14-D-0003/0005

5b. GRANT NUMBER

5c. PROGRAM ELEMENT NUMBER

6. AUTHOR(S)

Bellman, Jacob
Stricklin, Daniela

5d. PROJECT NUMBER

5e. TASK NUMBER

5f. WORK UNIT NUMBER

7. PERFORMING ORGANIZATION NAME(S) AND ADDRESS(ES)

Applied Research Associates, Inc.
801 N. Quincy Street, Suite 700
Arlington, VA 22203

8. PERFORMING ORGANIZATION REPORT NUMBER

9. SPONSORING/MONITORING AGENCY NAME(S) AND ADDRESS(ES)

Nuclear Technologies Department, Attn: Dr. Blake
Defense Threat Reduction Agency
8725 John J. Kingman Road, Mail Stop 6201
Fort Belvoir, VA 22060-6201

10. SPONSOR/MONITOR'S ACRONYM(S)

DTRA J9NTSN

11. SPONSOR/MONITOR'S REPORT NUMBER(S)

DTRA-TR-16-059

12. DISTRIBUTION/AVAILABILITY STATEMENT

DISTRIBUTION A. Approved for public release: distribution is unlimited.

13. SUPPLEMENTARY NOTES

14. ABSTRACT

Exposure to burn and radiation elicit epithelial cell death in the small intestine, reducing the density of the gut barrier. A reduced epithelial lining can result in suppressed nutrient absorption, bacterial translocation and mortality. This report describes the development of a mathematical model of small intestine epithelial cell kinetics following acute radiation and burn combined injury. This model has been developed from an existing system which simulates dynamic response of the small intestine epithelial cells to acute radiation alone. The model has been modified for improved radiation response, and an addition to the model allows for thermal injury response. A murine model has been developed to aid in the development of the human model due to data limitations. This model provides valuable time-dependent estimations of small intestinal damage, which can be useful in various scenarios of casualty estimation.

15. SUBJECT TERMS

Acute Radiation, Burn, Combined Injury, Ordinary Differential Equations Model, Small Intestine, Crypt, Villus, Gastrointestinal

16. SECURITY CLASSIFICATION OF:			17. LIMITATION OF ABSTRACT	18. NUMBER OF PAGES	19a. NAME OF RESPONSIBLE PERSON
a. REPORT	b. ABSTRACT	c. THIS PAGE			Dr. Paul Blake, Ph.D.
U	U	U	U	64	19b. TELEPHONE NUMBER *(Include area code)* 703-767-3433

UNIT CONVERSION TABLE

U.S. customary units to and from international units of measurement*

U.S. Customary Units	Multiply by → / ← Divide by†		International Units
Length/Area/Volume			
inch (in)	2.54	$\times 10^{-2}$	meter (m)
foot (ft)	3.048	$\times 10^{-1}$	meter (m)
yard (yd)	9.144	$\times 10^{-1}$	meter (m)
mile (mi, international)	1.609 344	$\times 10^{3}$	meter (m)
mile (nmi, nautical, U.S.)	1.852	$\times 10^{3}$	meter (m)
barn (b)	1	$\times 10^{-28}$	square meter (m^2)
gallon (gal, U.S. liquid)	3.785 412	$\times 10^{-3}$	cubic meter (m^3)
cubic foot (ft^3)	2.831 685	$\times 10^{-2}$	cubic meter (m^3)
Mass/Density			
pound (lb)	4.535 924	$\times 10^{-1}$	kilogram (kg)
atomic mass unit (AMU)	1.660 539	$\times 10^{-27}$	kilogram (kg)
pound-mass per cubic foot (lb ft^{-3})	1.601 846	$\times 10^{1}$	kilogram per cubic meter (kg m^{-3})
Pound-force (lbf avoirdupois)	4.448 222		Newton (N)
Energy/Work/Power			
electron volt (eV)	1.602 177	$\times 10^{-19}$	joule (J)
erg	1	$\times 10^{-7}$	joule (J)
kiloton (kT) (TNT equivalent)	4.184	$\times 10^{12}$	joule (J)
British thermal unit (Btu) (thermochemical)	1.054 350	$\times 10^{3}$	joule (J)
foot-pound-force (ft lbf)	1.355 818		joule (J)
calorie (cal) (thermochemical)	4.184		joule (J)
Pressure			
atmosphere (atm)	1.013 250	$\times 10^{5}$	pascal (Pa)
pound force per square inch (psi)	6.984 757	$\times 10^{3}$	pascal (Pa)
Temperature			
degree Fahrenheit (^oF)	$[T(^oF) - 32]/1.8$		degree Celsius (^oC)
degree Fahrenheit (^oF)	$[T(^oF) + 459.67]/1.8$		kelvin (K)
Radiation			
activity of radionuclides [curie (Ci)]	3.7	$\times 10^{10}$	per second (s^{-1}‡)
air exposure [roentgen (R)]	2.579 760	$\times 10^{-4}$	coulomb per kilogram (C kg^{-1})
absorbed dose (rad)	1	$\times 10^{-2}$	joule per kilogram (J kg^{-1}§)
equivalent and effective dose (rem)	1	$\times 10^{-2}$	joule per kilogram (J kg^{-1}**)

*Specific details regarding the implementation of SI units may be viewed at http://www.bipm.org/en/si/.

†Multiply the U.S. customary unit by the factor to get the international unit. Divide the international unit by the factor to get the U.S. customary unit.

‡The special name for the SI unit of the activity of a radionuclide is the becquerel (Bq). (1 Bq = 1 s^{-1}).

§The special name for the SI unit of absorbed dose is the gray (Gy). (1 Gy = 1 J kg^{-1}).

**The special name for the SI unit of equivalent and effective dose is the sievert (Sv). (1 Sv = 1 J kg^{-1}).

This page is intentionally left blank.

Table of Contents

Table of Contents i

List of Figures iii

List of Tables iv

Acknowledgements v

Executive Summary 1

1 Introduction 2
- 1.1 Modeling Gastrointestinal Cell Kinetics 2
- 1.2 Model Implementation 2
- 1.3 Existing Mathematical Models 2

2 Methods 4
- 2.1 Murine Model Parameterization 4
- 2.2 Human Model Parameterization 5
- 2.3 Optimization for Parameter Fitting 5

3 Modeling the Small Intestine 6
- 3.1 Biological Description 6
- 3.2 Mathematical Model 7
- 3.3 Radiation Injury 9
- 3.4 Thermal Injury 10
- 3.5 Experimental Data 11
  - 3.5.1 Biological Data Used to Inform Parameters 11
  - 3.5.2 Radiation and Burn Data 15
  - 3.5.3 Additional Parameter Bounds 19
- 3.6 Parameterization Results 20
  - 3.6.1 Murine Radiation Experiments 20
  - 3.6.2 Human Radiation Experiment 23
  - 3.6.3 Murine Burn Experiments 24

4 Combined Injury 25
- 4.1 Simulation of Murine Data 25
- 4.2 Simulating the Human Model 27

5 Future Work 30
- 5.1 Parameter Analysis 30
- 5.2 Alternative Modeling Approaches 30
- 5.3 Correlating Model Outputs with Clinical Endpoints 30

5.4 Modeling Additional Insults . . . 31

6 Conclusion . . . 32

References . . . 33

7 Abbreviations, Acronyms and Symbols . . . 37

Appendix A Mathematical Model of the Small Intestine Cell Kinetics . . . 38

Appendix B Supplementary Figures . . . 41

B.1 Additional Rodent Insult Experiments . . . 41

B.2 Rodent Radiation Experiments . . . 43

B.3 Villus Height and Cell Count . . . 52

Appendix C Human Extrapolation . . . 53

List of Figures

3.1 Diagram of crypt and villus structure and epithelial cell dynamics. 6
3.2 A diagram of the small intestine cell kinetic model with burn and radiation responses. 7
3.3 Murine data from acute radiation experiments (0 to 6 Gy). 15
3.4 Murine data from acute radiation experiments (6 to 8 Gy). 16
3.5 Murine data from acute radiation experiments (8 to 25 Gy). 16
3.6 Simulations of a murine radiation experiments (0 to 6 Gy). 21
3.7 Simulations of a murine radiation experiments (6 to 8 Gy). 21
3.8 Simulations of a murine radiation experiments (8 to 25 Gy). 22
3.9 Simulation of a human radiation therapy experiment. 23
3.10 Simulations of villus cells from rodent burn experiments. 24
3.11 Simulations of crypt cells from rodent burn experiments. 24

4.1 Simulations of the Baker and Valeriote, 1968 combined injury murine experiment. 25
4.2 Simulations of the Carter et al., 2014 combined injury murine experiment. . . . 26
4.3 Simulations of the Nesterenko and Piskarev, 1983 combined injury murine experiment. 26
4.4 Combined injury simulations of villus cells with the human model. 28
4.5 Combined injury simulations of crypt cells with the human model. 29

B.1 Simulations of non-radiation rodent insult experiments. 42
B.2 Simulations of the Galjaard and Bootsma, 1969 and Galjaard et al., 1972 experiments. 43
B.3 Simulations of the Kononenko and Farafonov, 1969 experiments. 44
B.4 Simulations of the Matsuzawa and Wilson, 1965 experiments. 45
B.5 Simulations of the Matsuzawa et al., 1973 experiments. 46
B.6 Simulations of the Patel et al., 2012 experiments. 47
B.7 Simulations of the Potten and Loeffler, 1990 experiments. 47
B.8 Simulations of the Quastler, 1956 experiments. 48
B.9 Simulations of the Rijke, 1977 experiments. 49
B.10 Simulations of the Sato et al., 1972 experiments. 50
B.11 Simulations of the Sherman and Quastler, 1960 experiment. 50
B.12 Simulations of an experiment reported in Smirnova, 2010. 51
B.13 Plot of villus height against villus counts measured in Rijke, 1977. 52

C.1 Crypt cell simulations for human and murine models responding to radiation and burn. 54
C.2 Villus cell simulations for human and murine models responding to radiation and burn. 55

List of Tables

3.1 References and bounds for cellular measurements in the murine small intestine. . 12
3.2 Murine parameter associations with experimental measurements. 12
3.3 References and bounds for cellular measurements in the human small intestine. . 13
3.4 Human parameter associations with experimental measurements. 14
3.5 Optimization data for the irradiated murine small intestine model. 15
3.6 Estimated dosing regimen for the Trier and Browning, 1966 experiment. 17
3.7 Burn data simulated by the murine small intestine model. 18
3.8 Additional parameter bounds. 19

A.1 Biological descriptions, parameters and variables in the small intestine mathematical model. 38
A.2 Murine and human parameters. 40

C.1 Extrapolated human burn parameters 53

Acknowledgements

The content presented in this report would not have been possible without the efforts of many talented and dedicated researchers. The authors are grateful for the technical developments of Dr. Olga Smirnova, who constructed the foundation of the radiation model used for this modeling effort, and Ms. Jacqueline Wentz and Dr. Darren Oldson, who made considerable improvements to Smirnova's model. This work would not be possible without the many experimentalists who produced the data used to parameterize and validate our models. We also gratefully acknowledge Dr. Paul Blake and DTRA's Nuclear Technologies Survivability for programmatic support; the work was performed under DTRA contract HDTRA1-14-D-0003; 0005.

Executive Summary

This report is part of an ongoing effort to develop computer models of human response to combined injuries anticipated after a nuclear detonation. The following study describes improvements and extensions of a mathematical model of the small intestine epithelium. The model is designed to simulate small intestine crypt and villus cellular populations following exposure to acute radiation and thermal injuries. This information can be used to quantify damage of the epithelial lining of the small intestine.

Major results of this modeling effort include:

- A murine model has been optimized to a large set of radiation response data.
- A human model has been optimized to radiation response data.
- Burn effects of the murine model have been optimized against thermal injury data.
- Burn response of the human model has been extrapolated from the murine model.
- The murine model has been validated with radiation and burn combined injury data.

1 Introduction

Applied Research Associates, Inc. (ARA) has been tasked by the Defense Threat Reduction Agency (DTRA) to support its mission to safeguard the United States against weapons of mass destruction (WMDs). ARA supports this effort by developing state–of–the–art mathematical models that predict medical and performance effects of radiation and burn injuries, thereby enhancing our understanding of the potential impact of a nuclear detonation.

1.1 Modeling Gastrointestinal Cell Kinetics

Radiation and burn injuries affect the cellular composition of the epithelial lining of the small intestine. A reduced epithelial lining results in nutrient absorption insufficiencies and permeability changes. Understanding the cellular kinetics of small intestine epithelial cells will aid in predicting and analyzing casualties. To this end, we developed mathematical models of the cellular kinetics of the small intestine in response to radiation, burn and combined injuries. Murine models have been constructed to assist with human model development.

1.2 Model Implementation

The models developed in this report are being implemented in HENRE (Health Effects from Nuclear and Radiological Environments), a user–friendly software platform with which one can (1) define an insult, (2) run models to predict health effects of that insult, and (3) analyze model output.

1.3 Existing Mathematical Models

There are a number of mathematical models of the small intestine that quantify the effects of radiation. Of these models, two stand out in particular. Russian scientist Olga Smirnova has developed a mathematical model that simulates three cellular compartments of the small intestine epithelium: proliferating crypt cells, maturing crypt cells and villus cells (Smirnova, 2010). The model is structured as a system of ordinary differential equations (ODEs) with nonlinear proliferation and feedback effects. Radiation is assumed to damage a portion of the proliferative cells in this model using the one-target-one-hit theory of cell damage (Lea, 1955)

Another powerful model of small intestine epithelial response is built into the Radiation-Induced Performance Decrement (RIPD) model (Anno et al., 1989, Anno et al., 1991). RIPD, a physiologically-based mathematical model of the effects of ionizing radiation, calculates time-dependent symptoms and predicts performance following exposure to irradiation. The gut injury model (GIM), which is built into RIPD, measures the effects of ionizing radiation on the small intestine epithelial lining. This model is nested into three components:

the lethal and potentially lethal (LPL) model (Curtis, 1986) calculates probabilities of survival for irradiated cells; the proliferation and intracellular repair (PAIR) model determines proliferation rates and mitotic delay from the LPL outputs; and a compartmental model determines the number of clonogenic cells, transit cells and villus cells from the LPL.

Compared to Smirnova's model, the GIM's quantification of DNA damage and DNA repair is more detailed than the cellular damage component of Smirnova's model. This detail is particularly useful for simulating protracted exposure, as the time components of damage and repair are crucial for capturing dose response for various dose rates. We are currently concerned with the effects of acute radiation where exposure time is generally low, and dose rate is generally high, and thus Smirnova's model of cellular damage is sufficient. The GIM is currently built into HENRE and we can thus leverage its capabilities for future projects that may involve simulating intestinal response to protracted radiation exposures.

Smirnova's model is more detailed than the GIM at the cellular compartment level, as it includes more interactions and feedback effects. This granularity improves the recovery kinetics of the model, which are important for accurate assessment of an exposed individual. Smirnova's model also leverages more biological data to support values chosen for model parameters. We have made improvements to Smirnova's model for our study which include fitting the model to a large set of experimental data, and adding burn response, which is absent in Smirnova's original model.

There are additional models of the small intestine epithelium, each with downfalls and limitations. As discussed in Smirnova, 2010, these include a model which is unable to accurately capture cellular damage from radiation (Meineke et al., 2001), a model which requires a heavy amount of data to accurately capture radiation response (Tyazelova, 1988), and a model which is too complex to achieve reasonable parameter identification (Gozenbuk and Keirim-Markus, 1988).

2 Methods

The following section provides details of our parameterization approach, including cost function definitions and the optimization algorithm used for parameter fitting. We used different approaches for parameterizing the human and murine models because there is a large amount of rodent data and very little human data. The purpose of constructing the murine model is to assist the development of the human model through species-to-species parameter extrapolations.

2.1 Murine Model Parameterization

Here, we describe our approach for parameterizing the murine small intestine model. We initially found biological measurements of mice including cell counts, migration rates, cell cycle times, etc. Accounting for variability in the data, we set ranges for parameters directly dependent on these measurements. This is discussed in more detail in Section 3.5.

After exhausting available biological measurements to inform parameter bounds, we fit model parameters, excluding those involved in burn response, to 25 experimental time series datasets. This data includes 21 radiation response datasets (Section 3.5.2) and four datasets of response to insults other than radiation or burn (Section B.1). All parameters, excluding those involved in burn response, were fit to this data using an optimization algorithm described in Section 2.3. During optimization, parameter bounds for biologically supported parameters were enforced, and large ranges were allowed for parameters lacking prior knowledge. The following cost function, C_m, was used to determine the difference between murine model simulations with a parameter set p, and the 25 time series datasets:

$$C_m(p) = \sum_{i=1}^{25} E_i(p). \tag{2.1}$$

The error from simulating each time series, E_i, is calculated as an average of absolute residuals between the time-dependent experimental data ((t_1, d_1), ..., (t_n, d_n)) and the trajectory of the corresponding simulated variable ($v(t)$):

$$E(p) = \frac{1}{n} \sum_{i=1}^{n} |d_i - v(t_i)|. \tag{2.2}$$

We use the sum of the absolute residuals, as opposed to the more conventional sum of squared errors, to measure error in this study for multiple reasons. For one, defining the cost function with the sum of squared errors assumes that the errors are normally distributed, which is not necessarily true here. Also, the data is diverse and is expected to contain outliers due to the diversity of experimental procedures. For instance, the data used for the murine model are from various sections of the small intestine and multiple species (rats and mice). By

using the absolute residuals, we place less emphasis on outliers of the data than we would with squared errors.

Burn response was implemented in the murine model by adding functions constructed from empirical evidence. More detailed biological data is required to model this response mechanistically. The parameters added to the model from these functions were fit to experimental time series data using the same optimization algorithm used to fit the first set of parameters. Much less data was available to fit the burn parameters (2 time series datasets, as opposed to 25).

2.2 Human Model Parameterization

Similar to our approach with the murine model, we first used experimental measurements to justify boundaries for as many parameters in the human model as possible (see Section 3.5 for details).

We defined the cost function differently for the human parameterization due to the fact that we only found one time series dataset which we could simulate with the model. The cost function for the human model C_h, dependent on the parameter set, p, compares the normalized epithelial data from Trier and Browning, 1966, where 13 epithelial measurements are taken over the course of radiation treatment ((t_1, d_1), ..., (t_m, d_m), m=13) to $\tilde{z}(t)$, the simulated normalized villus cell counts. This cost function places extra emphasis on simulating the nadir of the data set, which occurs at (t_8, d_8):

$$C_h(p) = E(p) + E_n(p), \tag{2.3}$$

where errors from simulating the average data point (E) and the nadir (E_n) are defined below:

$$E(p) = \frac{1}{m}\sum_{i=1}^{m} |\tilde{z}(t_i) - d_i|, \tag{2.4}$$

$$E_n(p) = |\tilde{z}(t_8) - d_8|. \tag{2.5}$$

We place particular emphasis on the nadir of the human data, which we calculate in both of the expressions above, and thus has weight $\frac{m+1}{m}$. We believe the nadir of the cell counts to be an important biomarker for the health of an exposed individual.

2.3 Optimization for Parameter Fitting

When searching for an optimal parameter set to best fit data, we solve the model using the "ode" function of the deSolve package (Soetaert et al., 2015) in the statistical computing environment R (R Core Team, 2013). We define the cost function using the modCost tool in the Flexible Modelling Environment (FME) library (Meysman et al., 2008), and we perform optimization using the DEoptim tool in the Global Optimization by Differential Evolution library (Ardia et al., 2015). DEoptim uses the standard search algorithm known as differential evolution (DE), to search parameter space for a global optimal parameter set.

3 Modeling the Small Intestine

This section provides biological and mathematical details of the cellular kinetic model of the small intestine. Following a description of the model, we present the data simulated by the model and provide simulation results of radiation and burn experiments.

3.1 Biological Description

The small intestine connects the stomach and the large intestine in the gastrointestinal tract. The small intestine is divided into three segments: the duodenum, the smallest segment which connects to the stomach; the jejunum, the largest segment; and the ileum, the final section connecting the jejunum to the large intestine.

The epithelial lining of the small intestine is composed of projections called villi. Multiple compartments located around the base of each villus, called crypts, supply the villi with epithelial cells. In humans, about five crypts supply each villus (Ferguson et al., 1977), while there are about 10 crypts per villus in mice (Wright and Irwin, 1982). Throughout the following report, we refer to the collection of a villus and its associated crypts as a column. Clonogenic cells located near the base of the crypts provide the column with new cells, which proliferate as they migrate up the crypts (Quastler and Sherman, 1959). Proliferating cells begin to mature as they reach their respective villus. Once on the villus, the cells (now referred to as villus cells) travel to the villus tip, where they are shed into the lumen of the intestine (Figure 3.1).

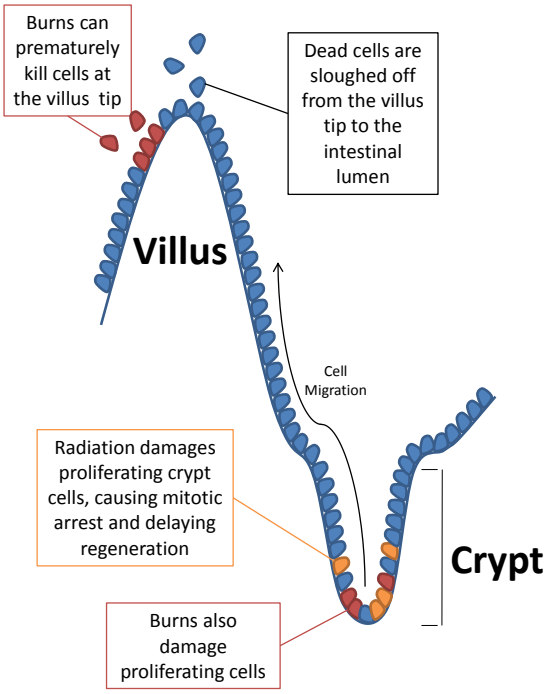

Figure 3.1: Diagram of crypt and villus structure and epithelial cell dynamics.

Radiation and burn injuries have an immediate effect on crypt and villus epithelial cells in the small intestine. Proliferating crypt cells respond to radiation by immediately initiating a mitotic delay, and many proliferating cells undergo apoptosis (Lesher, 1967, Bond et al., 1965). Burn has an immediate effect on villus cells, promoting early cell death before migration is complete (Carter et al., 2014, Wolf et al., 1999). This response is fast and strong but is not observed after two days in mice (Wolf et al., 1999). Crypt cells exhibit an additional response to burn which dampens proliferation. This secondary response has

been reported in mice no sooner than one day after burn, but persists for at least a week post-insult (Jeschke et al., 2007).

3.2 Mathematical Model

The following section describes the mathematical model of the small intestine we have developed for this study. Figure 3.2 provides a diagram of the model including the maturation and migration of the small intestine epithelial cells, feedback elements of the system, and the effects of radiation and burn. Negative feedback through the proliferation compartment from crypt and villus cells is modeled based on the chalone feedback reported in numerous cell lines by Bullough, 1971. In Smirnova, 2010, this feedback is assumed to depend on a mediator, promoted by crypt and villus cells, which inhibits crypt cell proliferation. Here, we modify this assumption, proposing that a generic mediator stimulates proliferation, but the level of this mediator is down-regulated by the crypt and villus cells. We have made this modification in anticipation of simulating drug applications which generally promote, rather than inhibit, cellular processes. Changing this assumption does not have a significant effect on the structure of the mathematical model. In addition to negative feedback through proliferation, there is also evidence that maturation rates through crypt and villus compartments are directly related to the rate of proliferation (Smirnova, 2010). We will discuss responses to radiation and burn in Sections 3.3 and 3.4, respectively.

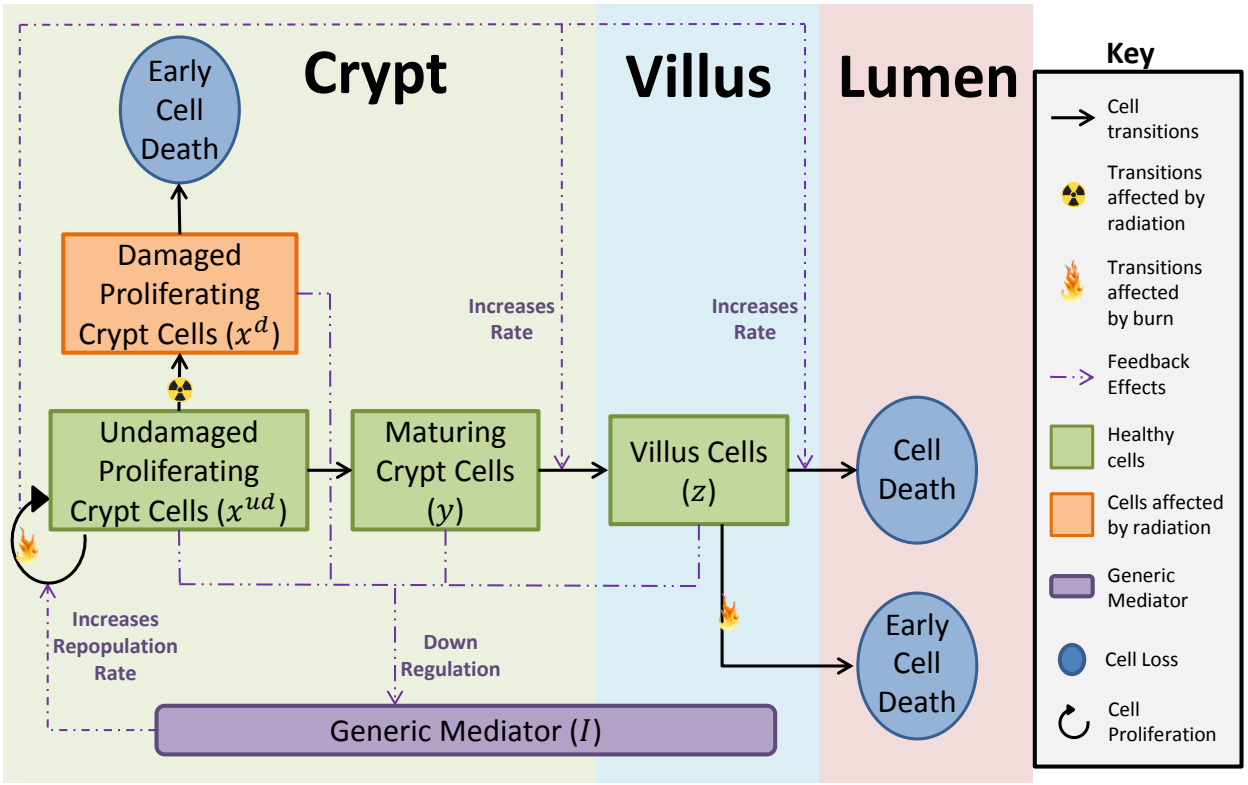

Figure 3.2: A diagram of the small intestine cell kinetic model with burn and radiation responses.

The complete mathematical model of the small intestine and a comprehensive list of variables, parameters, and parameter values are provided in Appendix A. The model is a set of ordinary differential equations, following the structure in Smirnova, 2010, tracking proliferating crypt cells (x), maturing crypt cells (y) and villus cells (z), each representing the number of cells per villus column. In the model, the generic mediator I is assumed to upregulate cellular proliferation (Equation 3.7). At the same time, each cell type is assumed to downregulate the mediator (Equation 3.4). The transit rates F for maturing crypt cells, and E for villus cells are assumed to be linearly dependent on the proliferation rate B, as seen in Equations 3.5 and 3.6. This is based on experimental evidence that suggests both independent and dependent transit rates for both cell types (Smirnova, 2010).

Equations of the model, excluding radiation and burn effects, are provided below:

$$\dot{x} = Bx - \gamma x \tag{3.1}$$
$$\dot{y} = \gamma x - Fy \tag{3.2}$$
$$\dot{z} = Fy - Ez \tag{3.3}$$
$$\dot{I} = G - H(x + \theta y + \vartheta z)I \tag{3.4}$$
$$F = \delta(1 + LB) \tag{3.5}$$
$$E = \psi(1 + MB) \tag{3.6}$$
$$B = \frac{\alpha}{1 + K/I}. \tag{3.7}$$

In the above equations, the following are constant: γ, G, H, θ, ϑ, δ, L, ψ, M, α and K. Assuming mediator interactions occur on a fast time scale, we solve for I using a quasi-steady-state approximation. Setting $\dot{I} = 0$ in Equation 3.4 gives us the following:

$$I = \frac{G}{H(x + \theta y + \vartheta z)}. \tag{3.8}$$

Substituting Equation 3.8 into Equation 3.7,

$$B = \frac{\alpha}{1 + \beta(x + \theta y + \vartheta z)} \tag{3.9}$$

where

$$\beta = \frac{HK}{G} \tag{3.10}$$

Compared to the model structure of Smirnova, 2010, it is clear that changing the mediator effect from inhibitory to stimulatory only affects the definition of the constant β.

At equilibrium, $\dot{x} = \dot{y} = \dot{z} = 0$, $x = \bar{x}$, $y = \bar{y}$ and $z = \bar{z}$. Assuming $\bar{x} > 0$, $\bar{y} > 0$, and $\bar{z} > 0$, the following equations represent the relative equilibrium compartment sizes (using

Equations 3.1 - 3.3):

$$\bar{x} = \frac{\alpha/\gamma - 1}{\beta(1 + \frac{\theta\gamma}{\delta(1+L\gamma)} + \frac{\vartheta\gamma}{\psi(1+M\gamma)})} \tag{3.11}$$

$$\bar{y} = \bar{x}\frac{\gamma}{\delta(1 + L\gamma)} \tag{3.12}$$

$$\bar{z} = \bar{x}\frac{\gamma}{\psi(1 + M\gamma)}. \tag{3.13}$$

We use normalized numbers of crypt and villus cells to simulate normalized experimental data. For this reason, we normalize the variables of the mathematical model, which we express as $\widetilde{x}$, $\widetilde{y}$ and $\widetilde{z}$. A non-dimensionalization of the model variables can be found below:

$$\dot{\widetilde{x}} = \gamma\widetilde{x}(\widetilde{B} - 1) \tag{3.14}$$

$$\dot{\widetilde{y}} = \delta\left((1 + l)\widetilde{x} - (1 + l\widetilde{B})\widetilde{y}\right) \tag{3.15}$$

$$\dot{\widetilde{z}} = \psi\left(\frac{1 + m}{1 + l}(1 + l\widetilde{B})\widetilde{y} - (1 + m\widetilde{B})\widetilde{z}\right), \tag{3.16}$$

where $l = \gamma L$, $m = \gamma M$ and $\widetilde{B} = B/\gamma$.

When simulating experimental data, we use $\widetilde{z}$ to represent the normalized number of villus cells per column. We simulate normalized crypt cells per column using the crypt cell mass ($CCM = \frac{x + y}{\bar{x} + \bar{y}}$). This can be expressed in terms of the normalized variables:

$$CCM = \frac{\delta(1 + l)\widetilde{x} + \gamma\widetilde{y}}{\delta(1 + l) + \gamma}. \tag{3.17}$$

Similarly, we can express the normalized total number of epithelial cells, or epithelial mass ($EM = \frac{x + y + z}{\bar{x} + \bar{y} + \bar{z}}$), in terms of normalized variables:

$$EM = \frac{\psi\delta(1 + l)(1 + m)\widetilde{x} + \gamma\psi(1 + m)\widetilde{y} + \delta\gamma(1 + l)\widetilde{z}}{\psi\delta(1 + l)(1 + m) + \gamma\psi(1 + m) + \delta\gamma(1 + l)}. \tag{3.18}$$

3.3 Radiation Injury

Following exposure to radiation, proliferating crypt cells become damaged and die by apoptosis (Potten and Grant, 1998). Following the structure of the model in Smirnova, 2010, we account for this damage by dividing the proliferation compartment into damaged (x^d) and undamaged (x^{ud}) cellular sub-compartments ($x = x^{ud} + x^d$). We assume an immediate cellular exchange from undamaged to damaged compartments, simulating dose response with a multitarget single-hit model (Joiner, 2009). This theory proposes that one hit of radiation in n different sensitive DNA regions (targets) is required to kill a radiosensitive cell. In response to a dose of D Gy at $t = 0$, we set initial values of x^{ud} and x^d to the following:

$$x^d(0) = \bar{x}(1 - e^{-D/D^0})^n \tag{3.19}$$
$$x^{ud}(0) = \bar{x}(1 - x^d(0)) \tag{3.20}$$

where the parameters D_0 and n determine the degree of the dose response. We assume the damaged cells die at an average rate of ν, but these cells can feed back through a mediator to inhibit proliferation. ϕ represents the strength of this feedback, relative to the strength of feedback by undamaged cells. Updating the rate of proliferation to reflect this:

$$B = \frac{\alpha}{1 + \beta(x^{ud} + \phi x^d + \theta y + \vartheta z)}, \tag{3.21}$$

and normalizing ($\widetilde{x}^{ud} = x^{ud}/\bar{x}$ and $\widetilde{x}^d = x^d/\bar{x}$), we find the following:

$$\widetilde{B} = \frac{\alpha/\gamma}{1 + b(\widetilde{x}^{ud} + \phi\widetilde{x}^d + \theta\widetilde{y}\dfrac{\gamma}{\delta(1+l))} + \vartheta\widetilde{z}\dfrac{\gamma}{\psi(1+m)})} \tag{3.22}$$

where

$$b = \frac{\alpha/\gamma - 1}{1 + \dfrac{\theta\gamma}{\delta(1+l)} + \dfrac{\vartheta\gamma}{\psi(1+m)}}. \tag{3.23}$$

3.4 Thermal Injury

There is very little data on human small intestine epithelial cell response to burn, but these effects have been documented in rodents. Multiple studies of mice and rats have reported that villus cells are quickly killed through apoptosis immediately following burn (Carter et al., 2014, Chen et al., 2013, Jeschke et al., 2007, Ramzy et al., 2000, Wolf et al., 1999). In mice, this response is strong and rapid, generally lasting less than two days (Wolf et al., 1999). In addition to villus killing, there is a delayed downregulation of crypt cell proliferation. In Jeschke et al., 2007, a 60% total body surface area (TBSA) burn in rats resulted in significant proliferation suppression that lasted for more than 7 days, while proliferation was observed to be normal one day after burn. We incorporate empirical functions in our model to account for these effects and fit the parameters of these functions to experimental data.

In our model, we simulate response to a burn of S% TBSA by modifying the rates of villus cell loss and cellular proliferation with functions $W_0(S,t)$ and $W_1(S,t)$, respectively:

$$\dot{x}^{ud} = (B - W_1(S,t))\, x^{ud} - \gamma x^{ud} \tag{3.24}$$
$$\dot{z} = Fy - (E + W_0(S,t))z \tag{3.25}$$

where

$$W_0(S,t) = \begin{cases} b_0 \dfrac{S}{S+k} \exp(-a_0 t) & t \geq t_b \\ 0 & t < t_b \end{cases} \tag{3.26}$$

$$W_1(S,t) = \begin{cases} b_1 \dfrac{S}{S+k} \exp\Big(- a_1 t(100 - S)\Big) & t > t_b + \Delta_b \\ 0 & t \leq t_b + \Delta_b \end{cases} \tag{3.27}$$

In Equations 3.24 - 3.27, $0 \leq S \leq 100$, t_b is the time of burn onset and Δ_b is the delay after burn before proliferation suppression begins. a_0 and a_1 determine the duration of the burn effects, b_0 and b_1 determine the maximum effects of burn, and k is an activation threshold for the burn effect. Assuming an equivalent proliferation suppression delay in mice and rats, we set $\Delta_b = 1$ day in the murine model, reflecting the results reported in Jeschke et al., 2007.

W_0 and W_1 have similar structures, where $b_i \dfrac{S}{S+k}, i = 0, 1$ represents the initial response to burn, and exponential functions are used to represent the relaxation of the burn responses. W_1 employs an additional dependence on burn size in the time component of the relaxation function to account for the fact that proliferation suppression lasts much longer for larger burns (Jeschke et al., 2007) than smaller burns (Baker and Valeriote, 1968, Carter et al., 2013, Wolf et al., 1999).

3.5 Experimental Data

The following section presents the data used in this study to parameterize and validate the human and murine small intestine models. As discussed in Section 2, our general approach for model parameterization is the following: utilize biological measurements of epithelial cells to inform as many parameters as possible, fit remaining unknown parameters (excluding those associated to burn response) to acute radiation data and fit the burn parameters to acute burn data. We have no human burn data, so we chose to extrapolate the human burn parameters from the murine model.

3.5.1 Biological Data Used to Inform Parameters

We have been able to leverage biological measurements of epithelial cell compartments and kinetics to inform a subset of parameters for the murine and human models. Table 3.1 lists biological measurements of epithelial cells in the murine small intestine, and Table 3.2 provides the relationships between these measurements and the model parameters. Using the information from Tables 3.1 and 3.2, we placed bounds on murine model parameters γ, α, δ, and ψ. We used the same approach for the human model, where Tables 3.3 and 3.4 list human biological measurements and their relationships to model parameters, respectively.

Table 3.1: References and bounds for cellular measurements in the murine small intestine.

Value measured	Intestinal Section	Reference	Lower	Upper
(E_0) Transit rate through villus compartment (d^{-1})	Jejunum	Wright and Irwin, 1982	0.506*	0.83*
(CP) Crypt population (cells/crypt)	Jejunum	Wright and Irwin, 1982	367.7*	525*
(GF) Growth fraction	Jejunum	Al-Dewachi et al., 1975	0.613$^{\diamond}$	0.65$^{\diamond}$
($CCPD$) Cells produced in crypt (cells/d)	Jejunum	Wright and Irwin, 1982	254*	394*
(MI_C) Crypt mitotic index (%)	Ileum	Matsuzawa and Wilson, 1965	2.88**	2.88**
	-	Smirnova, 2010	5.3$^{\diamond\diamond}$	5.3$^{\diamond\diamond}$
(T_M) Length of M phase (h)	Duodenojejunum	Wright et al., 1973	1.09†	1.31†
(T_S) Length of S phase (h)	Jejunum	Schultze et al., 1972	7.4$^{\diamond}$	8$^{\diamond}$

*Lower or upper bound for 95% CI.
**Only one measurement provided.
$^{\diamond}$Two values were calculated using different measuring techniques.
$^{\diamond\diamond}$ Original reference unknown.
† Human measurements, only two provided.

Table 3.2: Murine parameter associations with experimental measurements.

Parameter	Biological Meaning	Formula[§]
γ	Steady-state rate of proliferative compartment repopulation	$\frac{MI_C}{T_M * GF}$
α	Maximum rate of proliferative compartment repopulation	$1/(T_M + T_S)$
δ	Minimum transit rate through maturation compartment	$\frac{CCPD}{CP(1-GF)(1+l)}$
ψ	Minimum transit rate through villus compartment	$E_0/(1+m)$

[§]Experimental measurements: crypt mitosis index (MI_C), growth fraction (GF), crypt cells produced per day ($CCPD$), crypt population (CP), duration of M phase (T_M) and duration of S phase (T_S).

Table 3.3: References and bounds for cellular measurements in the human small intestine.

Value measured	Intestinal Section	Reference	Lower	Upper
(MI) Mitotic index (%)	Jejunum	Savidge et al., 1995	0.97*	1.05*
(PPC) Proliferating crypt cells (cells/crypt)	Jejunum	Savidge et al., 1995	521.3*	542.7*
(MPC) Maturing crypt cells (cells/crypt)	Jejunum	Savidge et al., 1995	114.7*	119.3*
(CPV) Crypts per villus	Jejunum	Ferguson et al., 1977	3.78*,†	6.5*,†
(VH) Villus height (μm)	Jejunum	Smit et al., 1986	427.9*	566.1*
(VHC) Villus height to cell count conversion (μm/cells)	Duodenum	Hasan and Ferguson, 1981	2.639*	3.679*
(T_M) Length of M phase (h)	Duodenojejunum	Wright et al., 1973	1.09**	1.31**
(T_S) Length of S phase (h)	Jejunum	Schultze et al., 1972	7.4$^\diamond$	8$^\diamond$

*Lower or upper bound for 95% CI.
**Only two measurements provided.
† Removed an outlier of 15.4.
$^\diamond$Measured in mice, two values were calculated using different measuring techniques.

Table 3.4: Human parameter associations with experimental measurements.

Parameter	Biological Meaning	Formula[§]
γ	Steady-state rate of proliferative compartment repopulation	(MI/T_M)
α	Maximum rate of proliferative compartment repopulation	$1/(T_M + T_S)$
δ	Minimum transit rate through maturation compartment	$\frac{\gamma * PPC}{MPC(1+l)}$
ψ	Minimum transit rate through villus compartment	$\frac{\gamma * PPC * CPV}{VHC * VH(1+m)}$

[§] Experimental measurements: mitosis index (MI), proliferating cells per crypt (PPC), maturing cells per crypt (MPC), crypts per villus (CPV), villus height (VH), villus height to cell count (VHC), duration of M phase (T_M) and duration of S phase (T_S).

3.5.2 Radiation and Burn Data

There is a large amount of time-dependent acute radiation data of crypt and villus cell counts from rodents (Table 3.5). We assume that normalized epithelial cell dynamics of mice and rats are the same and use this data to parameterize our murine model. In each study that reports the radiation dose as free-in-air (FIA), the reported doses have been converted to midline tissue (MLT) in Dant, 2016 using radiation and animal conversion factors. Our mathematical model simulates MLT radiation doses (Gy). For visualization purposes, we present this data in three radiation dose ranges: 0 to 6 Gy (Figure 3.3), 6 to 8 Gy (Figure 3.4), and 8 to 25 Gy (Figure 3.5).

Table 3.5: Optimization data for the irradiated murine small intestine model.

Reference	Measurements	Species	SI Section	MLT Dose (Gy)
Galjaard and Bootsma, 1969	C	Rat	Duodenum	3.17
Galjaard et al., 1972	C	Rat	Duodenum	5.55
Kononenko and Farafonov, 1969	C, V, E	Mouse	ns	7, 9
Matsuzawa and Wilson, 1965	C, V	Mouse	Ileum	26.14
Matsuzawa et al., 1973	C, V	Mouse	Duodenum	4.34, 17.34
Patel et al., 2012	C, V	Mouse	Jejunum	7.6
Potten and Loeffler, 1990	C	Mouse	Ileum	6.08
Quastler, 1956	V	Mouse	ns	1.74, 4.36, 17.43, 52.28
Rijke, 1977	C, V	Rat	Duodenum	2.38, 5.55
Sato et al., 1972	C, V	Mouse	Duodenum	8.71
Sherman and Quastler, 1960	C, V	Mouse	Ileum	25
Smirnova, 2010*	C, V	Mouse	ns	7

Note: C-crypt cells, V-villus cells, E-total epithelial cells, ns-not specified.
*Original reference unknown.

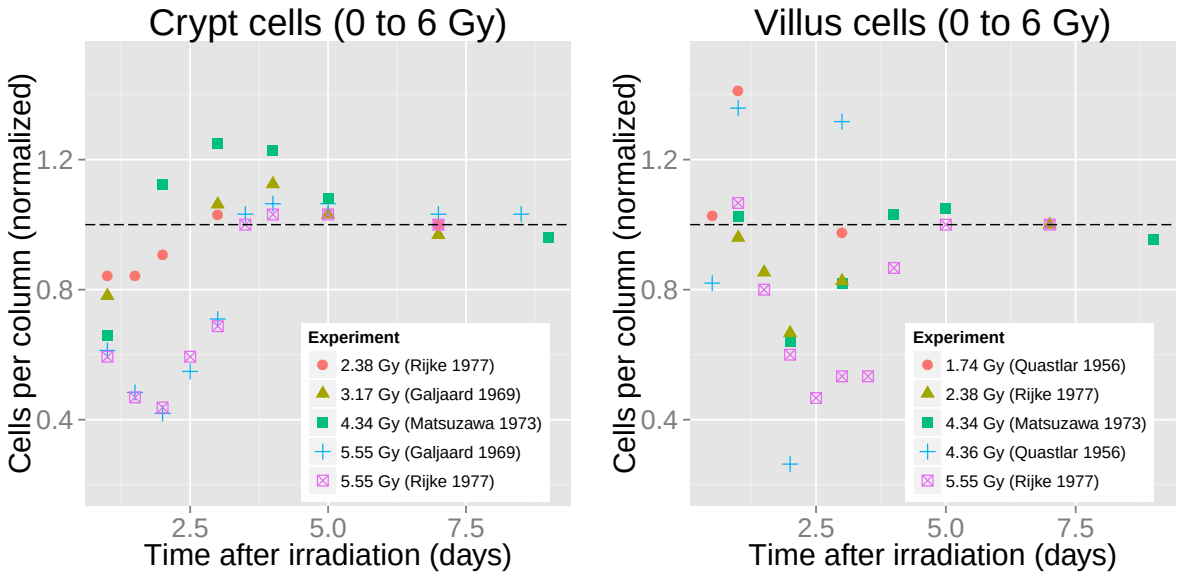

Figure 3.3: Murine data from acute radiation experiments (0 to 6 Gy).

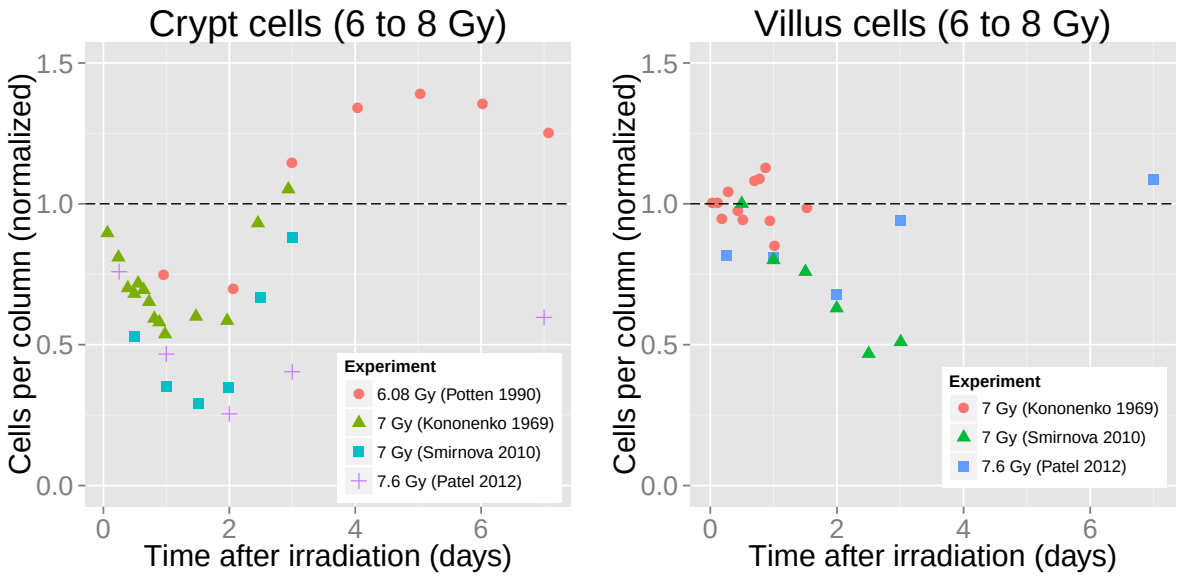

Figure 3.4: Murine data from acute radiation experiments (6 to 8 Gy).

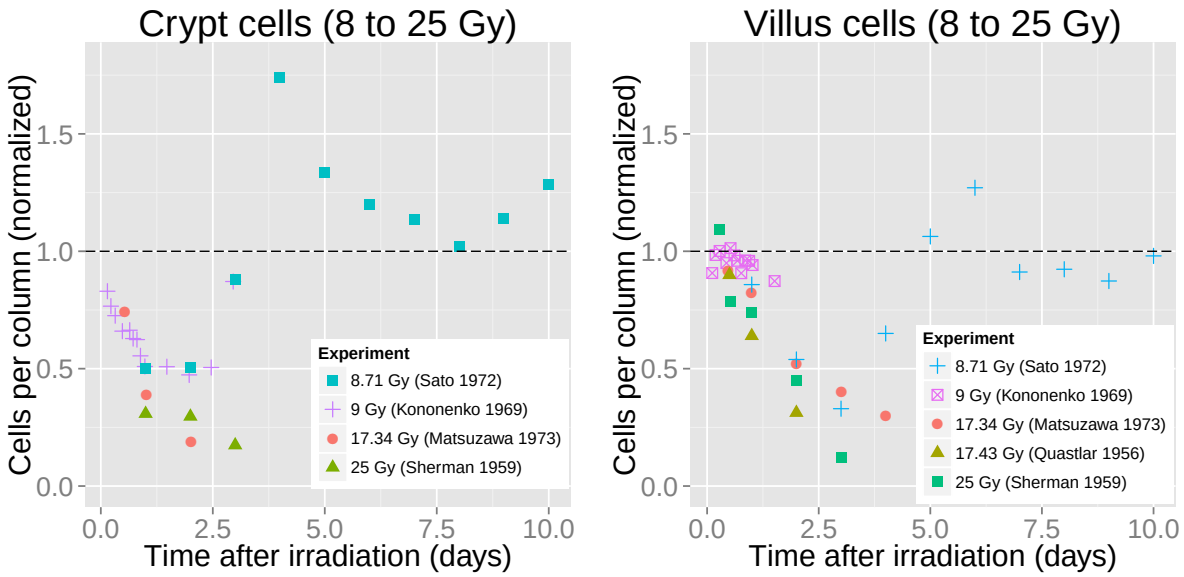

Figure 3.5: Murine data from acute radiation experiments (8 to 25 Gy).

Variability in data must be considered when comparing the model to the data. Measurement variability can be expected as we have collected data from studies with diverse experimental procedures. For instance, these datasets vary in histological measurement techniques, timing of measurements, species and dose estimation. As an example of variability in histological data, Smirnova, 2010 reports a crypt cell nadir approximately 70% below normal in response to a dose of 7 Gy (Figure 3.4), whereas no more than a 50% reduction of crypt cell counts are reported in response to a Dose of 8.71 Gy in Sato et al., 1972 (Figure 3.5).

We have only found one study that reports time-dependent human epithelial cell counts after radiation exposure (Trier and Browning, 1966). In Trier and Browning, 1966, crypt epithelial surface layer counts are reported during, and following, X-ray therapy for a clinical patient with seminoma (a germ cell tumor of the testicle). Unfortunately, the details of the timing and dosage of radiation treatments are not provided, other than total accumulated doses approximately 1, 5, 8, 15, 22 and 28 days after the start of treatment. In order to recreate the experiment *in silico*, we estimate the dosing regimen by assuming equally spaced treatments between each reported accumulated dose over the course of the 28-day trial. We have also converted the reported doses to MLT doses using a 0.96 conversion factor from roentgens (R) to Gy, and a 0.667 conversion factor from FIA to MLT for humans (Anno et al., 2003). Our estimated dosing regimen is provided in Table 3.6.

Table 3.6: Estimated dosing regimen for the Trier and Browning, 1966 experiment.

Time (d)	FIA Dose (R)	MLT Dose Received (Gy)
0	100 (0 R accumulated)	0.64
1.3	200 (100 R accumulated)	1.28
5.2	116.67 (300 R accumulated)	0.747
6.2	116.67	0.747
7.1	116.67	0.747
8.1	143.75 (650 R accumulated)	0.92
9.8	143.75	0.92
10.7	143.75	0.92
11.6	143.75	0.92
12.5	143.75	0.92
13.4	143.75	0.92
14.2	143.75	0.92
15.1	133.33 (1800 R accumulated)	0.853
16.3	133.33	0.853
17.4	133.33	0.853
18.6	133.33	0.853
19.7	133.33	0.853
20.8	133.33	0.853
22	140 (2600 R accumulated)	0.896
23.2	140	0.896
24.3	140	0.896
25.5	140	0.896
26.7	140	0.896
28	0 (3300 R accumulated)	0

Lastly, Table 3.7 lists the burn and combined burn and radiation experimental data we simulate with the murine model. We have found no human data measuring small intestine epithelial cellular response to burn. Due to a limited amount of data, we compare the murine model to normalized mouse and rat data, taken from any of the three small intestine segments (ileum, jejunum, duodenum). Although the model was developed in the context of the murine jejunum, we assume the normalized kinetics of the two species in each intestinal segment are the same.

A limited number of the rodent studies reported crypt and villus cell counts following thermal injury, and a few additional studies have measured villus height following burn.

According to rat data from Rijke, 1977, normalized villus height is approximately equal to normalized villus cell counts. To demonstrate this, we present data from Rijke, 1977 in Figure B.13, which reported villus lengths and villus cell counts after various radiation doses. This data demonstrates that normalized villus height is a reasonable approximation of normalized villus cell counts.

We use two of the time-series burn datasets to fit the burn-related parameters. In particular, we use the villus measurements after burn from Carter et al., 2014 and Jeschke et al., 2007. Using data with 15% and 60% TBSA, respectively allows the model to develop a dependence on % TBSA. The remaining burn, radiation and combined radiation and burn data is reserved for model validation.

Table 3.7: Burn data simulated by the murine small intestine model.

Reference	Cells	Data Use	Species	SI Section	Insult
Baker and Valeriote, 1968	C	Validation	Rat	D, I	16% TBSA + 7 Gy
	C	Validation	Rat	D, I	7 Gy
	C	Validation	Rat	D, I	16% TBSA
Carter et al., 2014	V	Validation	Mouse	I	15% TBSA + 4.72 Gy
	V	Validation	Mouse	I	4.72 Gy
	V	Optimization	Mouse	I	15% TBSA
Chen et al., 2013	V	Validation	Mouse	I	15% TBSA
Jeschke et al., 2007	V	Optimization	Rat	All	60% TBSA
Nesterenko and Piskarev, 1983*	C	Validation	Rat	na	15% TBSA + 5.5 Gy
	C	Validation	Rat	na	5.5 Gy
	C	Validation	Rat	na	15% TBSA

Note: C-crypt cells, V-villus cells, D-Duodenum, I-Ileum, na-not available, + indicates CI.
*Full translation unavailable.

3.5.3 Additional Parameter Bounds

Using the methods described in Section 2, we fit all parameters of the murine model (excluding those related to burn) to the data provided in Table 3.5. When fitting the parameters, we restricted γ, α, δ, and ψ to the narrow regions governed by the values and equations presented in Tables 3.1 and 3.2, respectively, and we allowed for a much larger range of mobility for the remaining parameters. Table 3.8 lists the bounds for the remaining parameters enforced when exploring parameter space for improved model accuracy of both human and murine models.

Table 3.8: Additional parameter bounds.

Parameter	Lower	Upper
θ	0.001	1000
ϑ	0.001	1000
l	1.5	2.5
m	1.5	2.5
D_0	1 Gy	10 Gy
n	1	10
ν	1 d^{-1}	10 d^{-1}
ϕ	0.001	1000
a_0	0.001	1000
a_1	0.001	1000
b_0	0.001	1000
b_1	0.001	1000
k	0.001	1000

We set the same bounds on each of the remaining parameters for both murine and human models. We restricted θ and ϑ to be in the interval [0.001, 1000], which allows feedback of maturing crypt and villus cells to be up to three orders of magnitude less than, or greater than, feedback provided by proliferating cells. l and m, feedback strengths of proliferation on maturation and villus transit rates, respectively, are each set to 2 in Smirnova, 2010, but we do not have access to the referenced study. We bound l and m in the interval [1.5, 2.5], allowing for a 25% adjustment of these values.

In Wentz, 2015, the multi-target, single-hit model was implemented to represent dose response. The dose response parameters (D_0 and n) were chosen to match experimental data approximated from Lesher and Lesher, 1970, which measured the number of crypt cells in synthesis post-radiation. Although this data is relevant, irradiated samples are rarely measured at the same time as controls, which makes it difficult to quantify the relative difference between experiment and control. Instead of using data from Lesher and Lesher, 1970, we fit the dose response parameters to time-course radiation data for both murine and human models, while placing moderate ranges (within one order of magnitude around the values chosen in Wentz, 2015) on both parameters (we bound D_0 and n in the interval $[1, 10]$).

The remaining radiation-related parameters, ν and ϕ, determine the duration and strength by which the damaged cells affect proliferation, respectively. ν was set to 2d^{-1} chosen in Smirnova, 2010, assuming average apoptosis lengths of 12 hours. In Potten and Grant, 1998, it was determined that the majority of apoptosis occurs within 3-6 hours of radiation, suggesting a faster rate of cell death. We chose to bound ν in the interval $[1, 10]$. We allow ϕ, the relative strength of feedback of the damaged cells on proliferation, the same freedom as θ and ϑ ($[0.001, 1000]$).

The burn-related parameters, a_0, a_1, b_0, b_1 and k, were fit to the rodent villus burn data in Carter et al., 2014 and Jeschke et al., 2007. Large ranges ([0.001, 1000]) were allowed for each of these parameters during optimization, as no prior knowledge was available for these parameters. Human values for these parameters are extrapolated from the murine model.

3.6 Parameterization Results

We now present model simulations of the experimental data used to optimize the radiation and burn kinetics of the small intestine model. Full details of the model are presented in Appendix A, including the human and murine parameters (Table A.2). Simulations of the models are presented against experimental data in Figures 3.6 - 3.11. When available, error bars are presented as $\pm$ standard deviations.

In addition to radiation and burn insults, we also simulated rat (Rijke et al., 1976) and mouse (Wright and Al-Nafussi, 1982) experiments, presented in Figure B.1. In Rijke et al., 1976, a method called villus clamping is used to interrupt the blood flow to the small intestine, causing an ischemic villus cell damage, killing villus cells without harming crypt cells. In Wright and Al-Nafussi, 1982, cytosine arabinoside is used to kill only proliferating crypt cells. Both of these experiments measure the dynamics of small intestinal cell recovery from insults other than radiation or burn.

3.6.1 Murine Radiation Experiments

Simulations of acute radiation rodent experiments are presented in Figures 3.6 - 3.8. In Section 3.5.2, we presented this data, delineated by dose and cellular measurement (Figures 3.3 - 3.5). Considering the variability in the data, the model is well suited for capturing each range of radiation dose. In particular, the model captures the time and value of villus nadir in a dose-dependent manner. The model is not as accurate when simulating crypt cells, but it is possible that this can be attributed to inconsistent data.

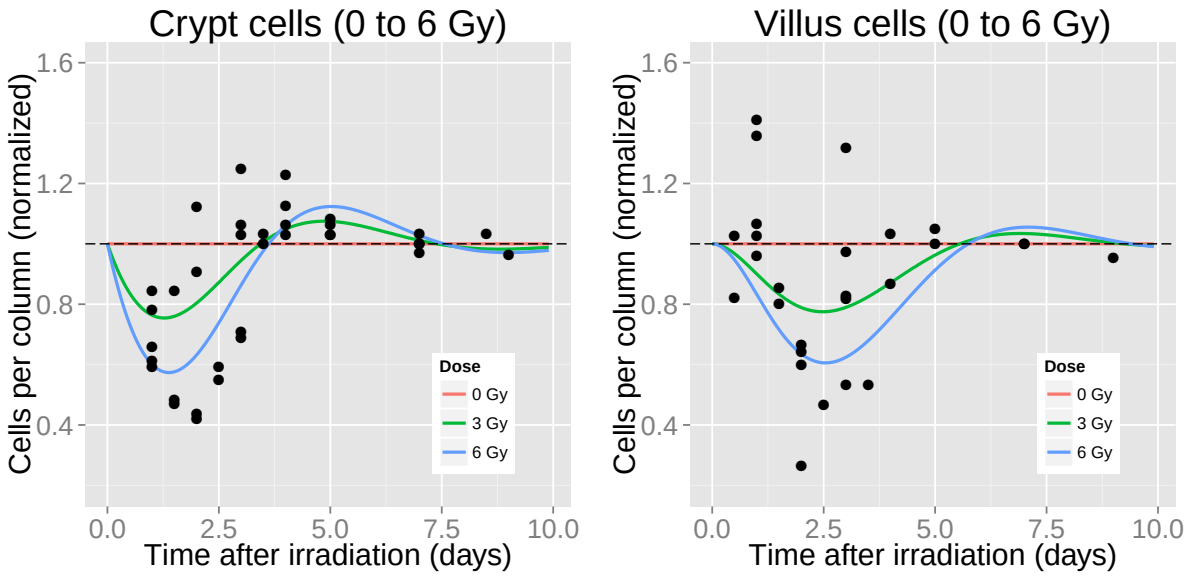

Figure 3.6: Simulations of a murine radiation experiments (0 to 6 Gy).

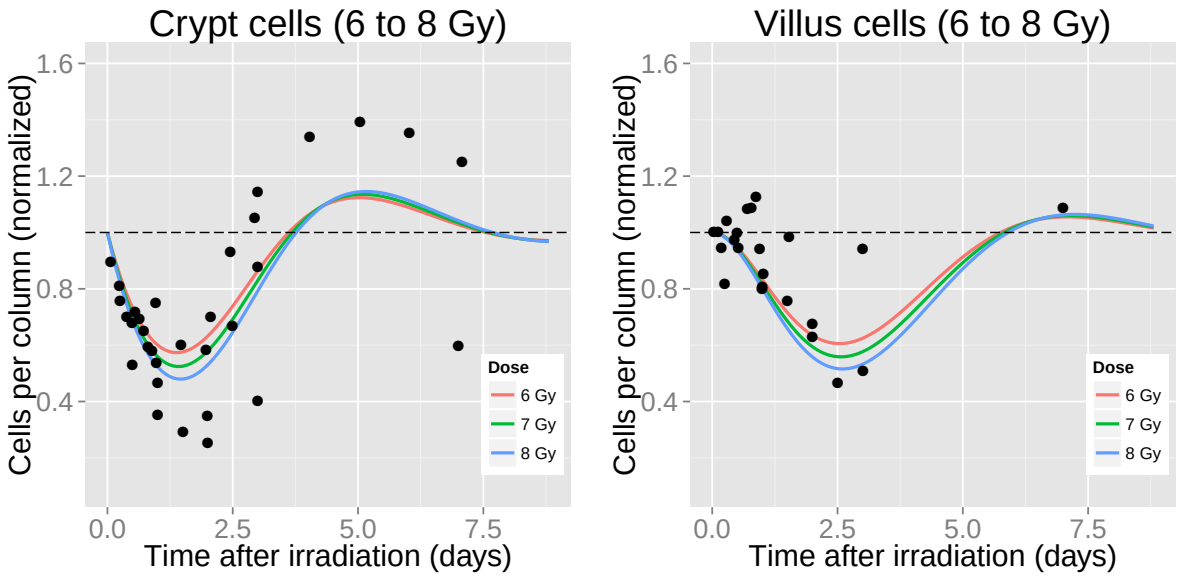

Figure 3.7: Simulations of a murine radiation experiments (6 to 8 Gy).

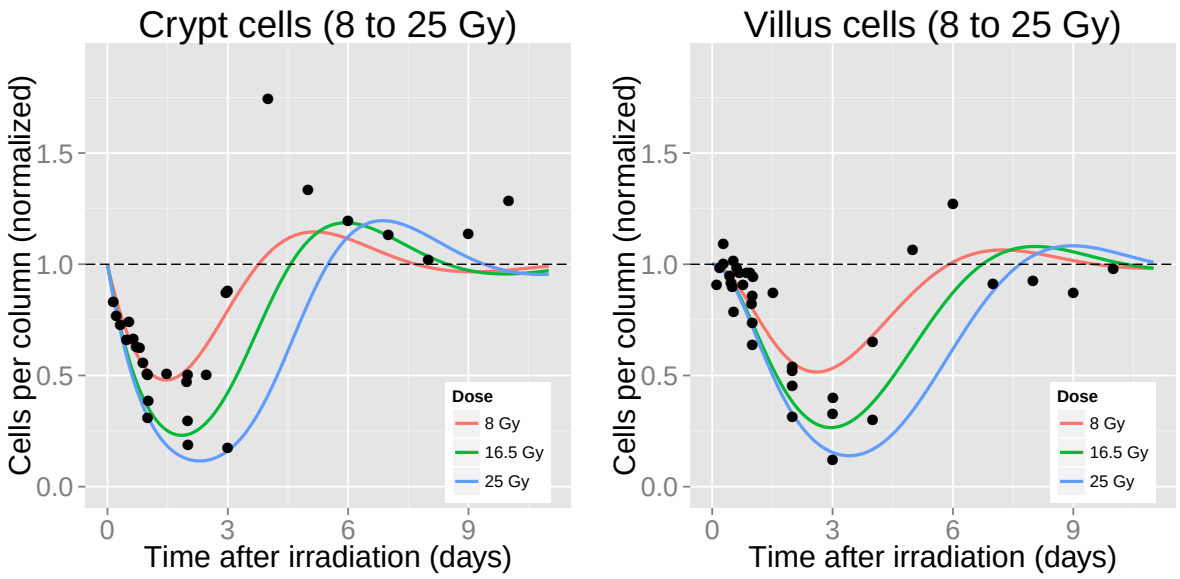

Figure 3.8: Simulations of a murine radiation experiments (8 to 25 Gy).

3.6.2 Human Radiation Experiment

Trier and Browning, 1966 is the only study we have found which reports time-dependent data of irradiated human epithelial cells. This data reports villus cell counts following repeat exposures of an unspecified dosing schedule, which we estimated (Table 3.6). Figure 3.9 provides the simulation of this data (red line), superimposed on the data (black triangles). An initial drop in cell counts is observed in the data, followed by a quick recovery about 12 days after the beginning of the treatment. The model is unable to capture this early recovery, but it is possible that this phenomenon is an artifact of measurement error. The model accurately captures the villus nadir, as well as the rate of recovery following the end of treatment.

The lack of adequate human data is the biggest limiting factor in firmly establishing human parameters for the model. Currently we have fit γ, α, δ, ψ, θ, ϑ, l, m, D_0, n, ν and ϕ to this single study, although γ, α, δ and ψ have been restricted to small ranges based on biological measurements. Allowing this many parameters to depend on one study of one individual places too much emphasis on this data. In the future, if we are unable to find more data of this nature, we will explore alternative approaches to parameterizing the human model.

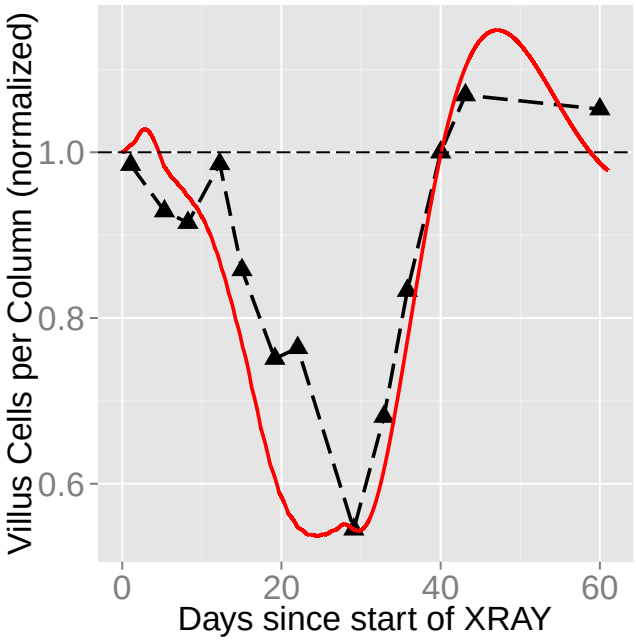

Figure 3.9: Simulation of a human radiation therapy experiment.

3.6.3 Murine Burn Experiments

In this section, we present simulations of burn response in the rodent small intestine. Figures 3.10 and 3.11 provide simulations of villus and crypt cell response to burn, respectively. In Chen et al., 2013, measurements were taken after two different drug vehicles were applied (gavage and i.p.), and in Baker and Valeriote, 1968, measurements were taken in two small intestine segments. The burn only data in Carter et al., 2014 and Jeschke et al., 2007 was used to optimize the burn-related murine parameters, and the remaining burn data serves to validate the model.

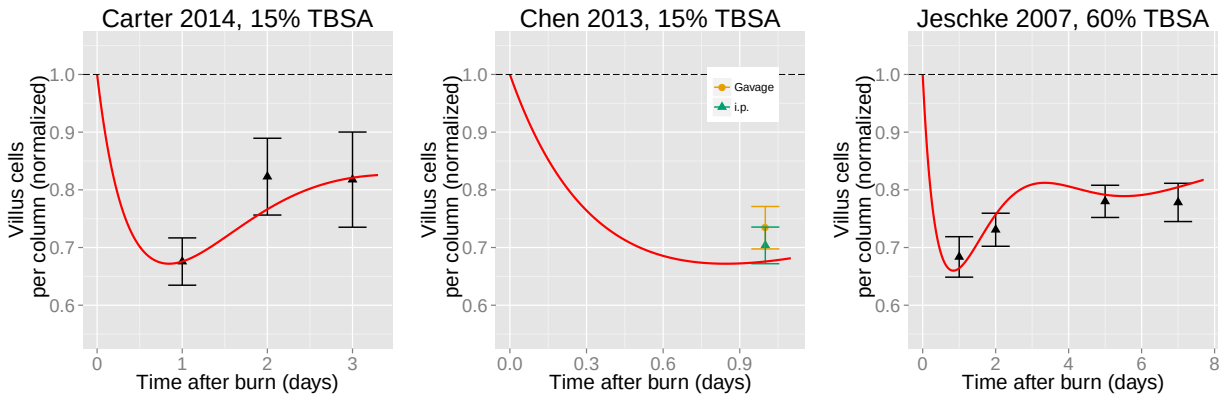

Figure 3.10: Simulations of villus cells from rodent burn experiments.

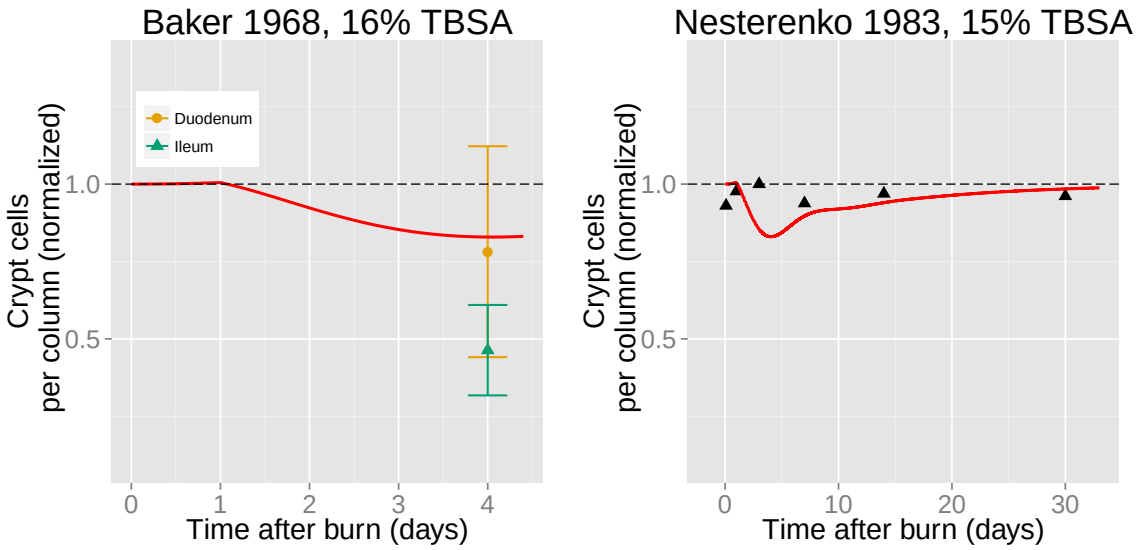

Figure 3.11: Simulations of crypt cells from rodent burn experiments.

4 Combined Injury

In the event of a nuclear weapon detonation, it is anticipated that there will be many casualties exposed to various ranges of acute radiation, burn, trauma, and other insults. It is therefore important that our models capture the synergistic effects of combined injuries. In this section, we present the ability of the mathematical model to reproduce combined radiation and burn injury experiments. The murine model is validated against experimental data, and the human model is simulated for various combinations of acute radiation and burn injuries.

4.1 Simulation of Murine Data

We have found three rodent experiments of combined radiation and burn which we can simulate with our model. Each of these experiments measured crypt or villus cells after radiation, burn and combined radiation and burn injuries. Figures 4.1 - 4.3 present simulations of each of these experiments against the experimental data.

In Baker and Valeriote, 1968, rat duodenum and jejunum crypt cells are measured four days after moderate burn, radiation or combined insults (Figure 4.1). There is a slight decrease in crypt cells four days after radiation, whereas the crypt cell population has recovered by this time in the case of burn and combined injuries. The model is able to capture each of these features.

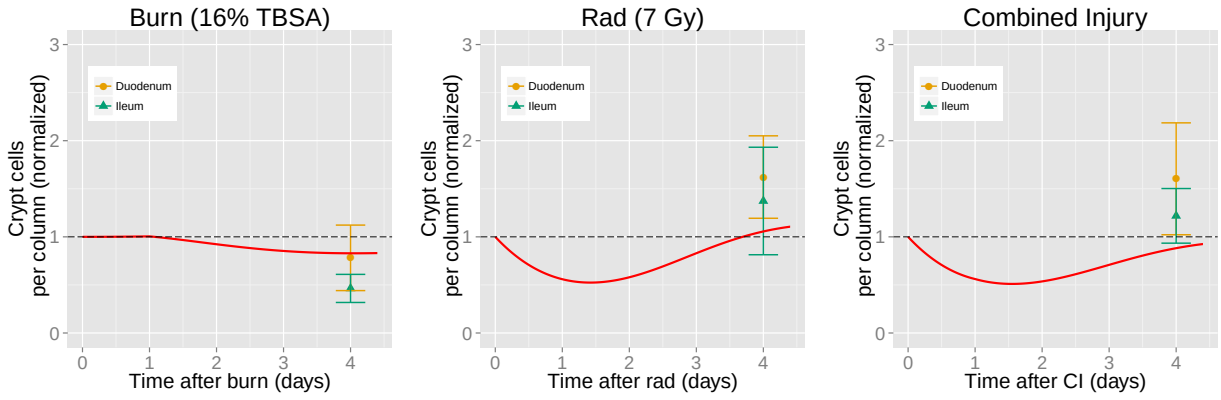

Figure 4.1: Simulations of the Baker and Valeriote, 1968 combined injury murine experiment.

The Carter et al., 2014 study measured villus cells 1, 2 and 3 days after radiation, burn and combined insults (Figure 4.1). The model captures the burn response of this experiment well, which is to be expected as this is one of the datasets used to fit the model. In response to radiation, there is a large reduction in villus cells (more than 30%), the extent of which is not reproduced by the model. Although the model does not capture the quick reduction in villus cells reported after radiation, the model is able to reproduce the attenuation of villus cell reduction from the combined injury. In particular, radiation and burn alone result

in an approximate 20% reduction in villus cells three days post-insult, whereas there is an approximate 40% reduction in villus cells three days after the combined injury.

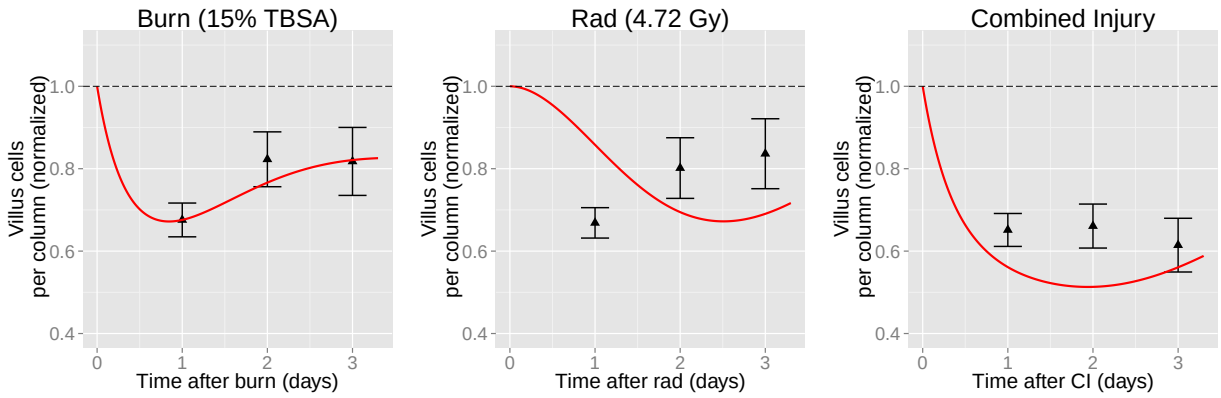

Figure 4.2: Simulations of the Carter et al., 2014 combined injury murine experiment.

In Nesterenko and Piskarev, 1983, moderate radiation, burn and combined insults are applied to rats before crypt cell measurements are taken 2 hours and 1, 3, 7, 14 and 30 days post-insult. For this data, we have not been able to acquire a full translation (Russian). It is possible that the 5.5 Gy reported in this experiment is FIA, and the MLT dose is smaller. In this case, our simulation may be an overestimate of the response, which could account for the large villus nadir following radiation only. The granularity in the reported measurements could also account for the differences in nadirs. For instance, it can be seen in Figures 3.3-3.5 that crypt cells reach their nadirs approximately two days after radiation. This could account for differences between nadirs, because the measurements in Nesterenko and Piskarev, 1983 are taken at 1 and 3 days post-radiation.

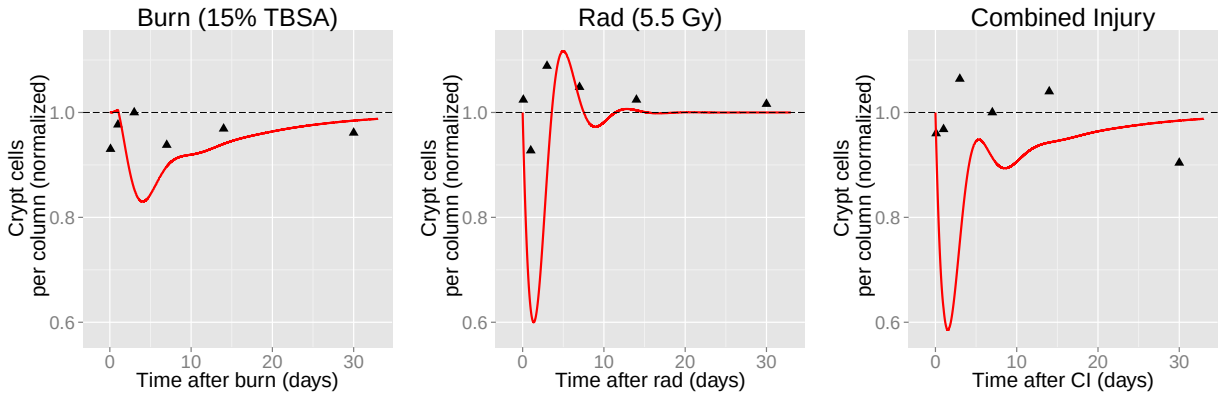

Figure 4.3: Simulations of the Nesterenko and Piskarev, 1983 combined injury murine experiment.

4.2 Simulating the Human Model

We have extrapolated human values of the burn-related parameters (a_0, a_1, b_0, b_1, k and Δ_b) from the murine model. Details of the parameter extrapolation are described in Section C. In short, the human burn parameters were fit to murine burn data, scaled in time and amplitude based on quantitative differences in human and murine radiation response. In Figures 4.4 and 4.5, we provide simulations of the human model exposed to various combinations of radiation and burn insults. As discussed with the murine model, the villus nadir has very little dependence on burn size, but the crypt cell proliferation is dampened. This human model provides simulations of human response to combined radiation and burn injury. Human burn and combined injury data is required to validate this model.

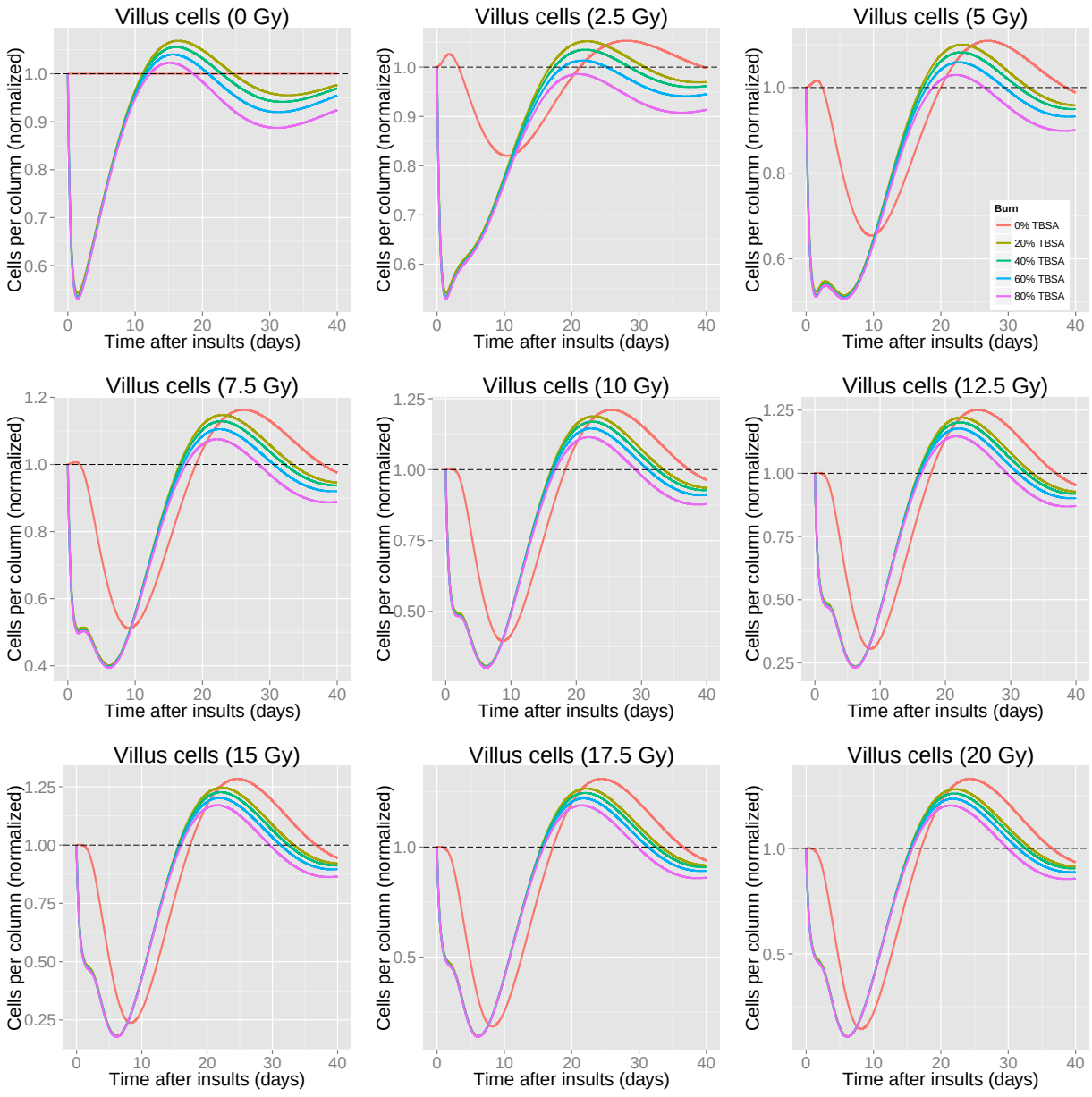

Figure 4.4: Combined injury simulations of villus cells with the human model.

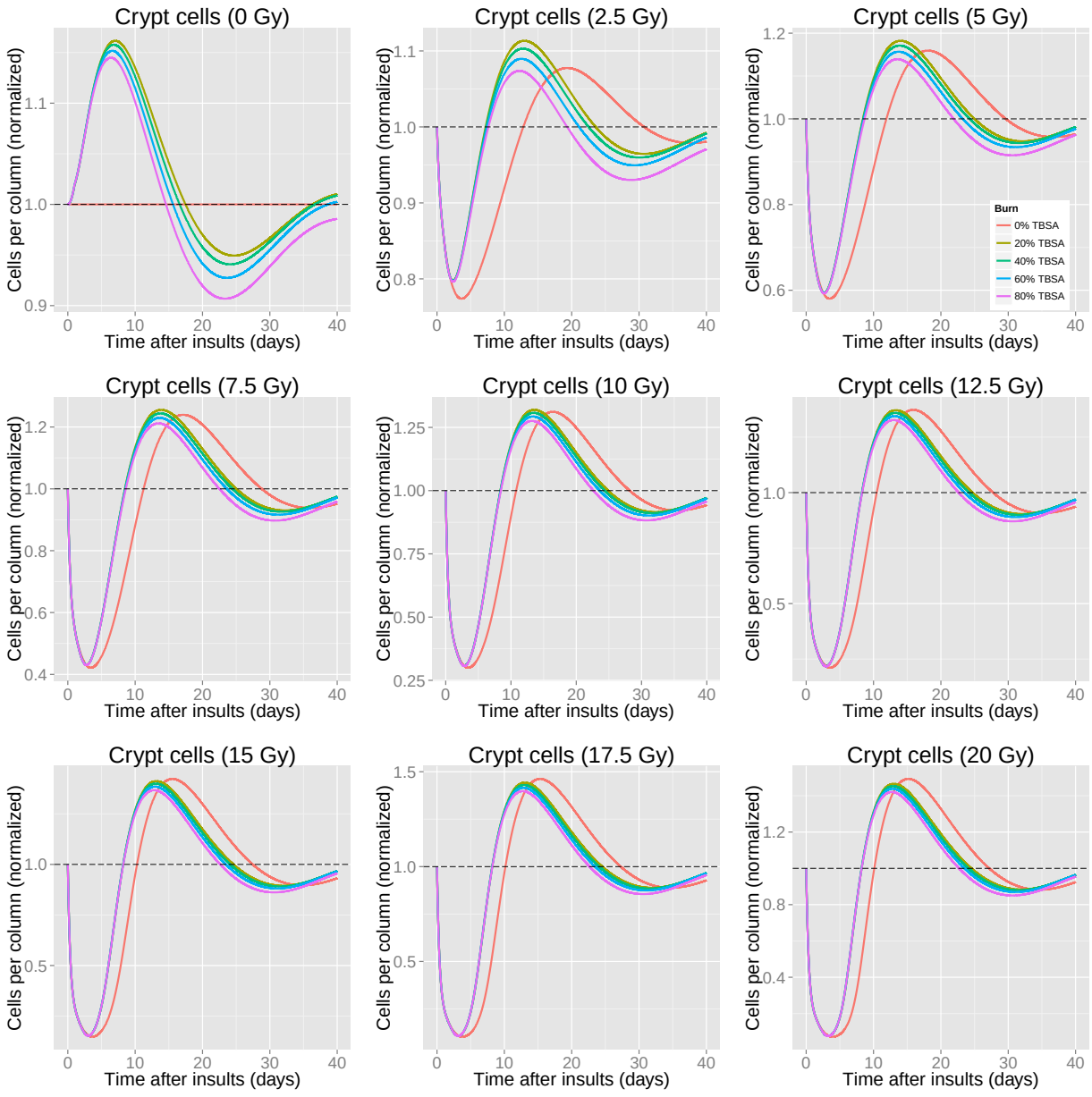

Figure 4.5: Combined injury simulations of crypt cells with the human model.

5 Future Work

We have developed mathematical models of the human and murine small intestine epithelial cells responding to radiation and burn combined injuries. This modeling project is an ongoing effort that can be improved with more data and alternative modeling techniques. This section discusses some of the advancements we plan to make to this model.

5.1 Parameter Analysis

Parameter sensitivity analysis and uncertainty analysis are important tools for understanding the inner workings of a model. These analysis techniques measure the dependencies of model outputs to parameter errors and uncertainties. A handful of methods have been developed to accurately and efficiently measure parameter sensitivities and uncertainties (Hamby, 1994). In the future, we plan to leverage these methods to analyze the parameters of our model. This information can be useful for detecting model error and examining biological anomalies.

5.2 Alternative Modeling Approaches

We will consider modeling other animals as a supplement to our current modeling approach. For instance, non-human primates (NHPs) have been studied in the context of radiation-induced gut injuries (MacVittie et al., 2012b, MacVittie et al., 2012a, Wang et al., 2015). We can use this data to build an NHP model of radiation response in the small intestine. There will be less data to parameterize an NHP model, but the extrapolation from NHP to human would be more reasonable than mice to humans.

Citrulline is an α-amino acid produced mainly by enterocytes in the small intestine mucosa and has been identified as an indicator of gut damage (Crenn et al., 2000). We could extend our current small intestine model to include the production of citrulline, dependent on the number of epithelial cells. This will allow us to leverage currently available human citrulline data. Furthermore, extending the small intestine model to include citrulline will increase the practicality of the model. Crypt and villus measurements require invasive procedures, whereas citrulline can be measured through plasma extraction. The use of citrulline as a biomarker can be beneficial for rapid patient analysis for injured patients.

5.3 Correlating Model Outputs with Clinical Endpoints

An upcoming project is to correlate hemodynamic, hematopoietic and small intestine kinetic models to clinical endpoints. For instance, we plan to correlate small intestine crypt and villus cell counts, following radiation and burn insults, to the probability of mortality and diarrhea. Depending on the available data, this will likely include measurements of crypt

and villus cell nadirs as thresholds for probability of mortality. There may be more high quality citrulline data, in which case we may reform our model to include citrulline produced from epithelial cells. We will compare our results to other models that have already made these correlations (Anno et al., 1991, for example).

5.4 Modeling Additional Insults

In addition to radiation and burn, we would like to include small intestine epithelial cell response to various types of trauma. In particular, we will include the effects of hemorrhagic shock on the intestinal mucosa, which has been studied in rats (Chang et al., 2005). Other effects we would like to model include blast overpressure, penetrating trauma and blunt trauma.

6 Conclusion

The small intestine is essential for nutrient absorption and is vulnerable to insults such as thermal injury and irradiation, which can deteriorate the epithelial lining of the small intestine, leading to increased risk of internal hemorrhaging, bacterial translocation, sepsis and mortality. The modeling efforts in this report support the DTRA mission, which aims at providing time-dependent casualty analysis given an arbitrary range, and combined injuries expected from a nuclear attack. It is important that these models are as accurate as possible when estimating casualties in a catastrophic event.

The mathematical models developed in this study are deterministic sets of ODEs, which capture the average effects murine and human epithelial cellular response to radiation, burn and combined injury. The murine model has been compared to mouse and rat data, collected from each of the three sections of the small intestine. Responding to radiation, the murine model captures the average of crypt and villus nadirs (Figures 3.6 - 3.8), which provide biomarkers for epithelial gut damage. We will also explore the idea of using a time element under a threshold as a biomarker for intestinal damage.

The human model is limited by the amount of data available. We have only collected one time-dependent dataset of irradiated human epithelial cells, and no data of human epithelial response to burn. We have parameterized the effects of burn in the human model by extrapolating from the murine model. We used mouse and rat data to parameterize the murine model, and the murine model compares well to available burn, and combined radiation and burn data. The aim of our approach is to improve the human model by supporting it with a well-developed and validated murine model. We hope to coordinate with experimentalists to gather more accurate, reliable and relevant data that can strengthen our model. Human data will still be a challenge to acquire since biopsies of the small intestine are invasive and rarely warranted in clinical studies. To address these limitations, we will explore alternative biomarkers of intestinal injury such as plasma citrulline, that may aid in extrapolating the impact of radiation on the GI tract.

In this study, we have developed a mathematical model capable of simulating combined radiation and burn injury response of small intestine cell kinetics. Data restrictions have provided challenges for parameterizing the human response to burn, but in the future we aim to use additional approaches for parameter calibration. The models developed in this report will be integrated in the health effects modeling software, HENRE.

References

Al-Dewachi HS et al. (1975). "Cell population kinetics in the mouse jejunal crypt". *Virchows Archiv. B: Cell Pathology* 18.3, pp. 225–242.

Anno GH et al. (1989). "Symptomatology of acute radiation effects in humans after exposure to doses of 0.5-30 Gy." *Health physics* 56.6, pp. 821–838.

Anno GH et al. (1991). Biological Effects of Protracted Exposure to Ionizing Radiation: Review, Analysis, and Model Development. Tech. rep. DNA-TR-90-157. Pacific-Sierra Research Corporation, Los Angeles, CA.

Anno GH et al. (2003). "Dose response relationships for acute ionizing-radiation lethality". *Health Physics* 84.5, pp. 565–575.

Ardia D et al. (2015). DEoptim: Global Optimization by Differential Evolution.

Baker DG and FA Valeriote (1968). "The effect of x-irradiation and thermal burn on the intestinal mucosa". *Canadian journal of physiology and pharmacology* 46.3, pp. 533–536.

Bond V, T Fliedner, and J Archambeau (1965). *Mammalian radiation lethality*. Academic.

Bullough WS (1971). "The actions of the chalones". *Agents and Actions* 2.1, pp. 1–7.

Carter SR et al. (2013). "Intestinal Barrier Disruption as a Cause of Mortality in Combined Radiation and Burn Injury:" *Shock* 40.4, pp. 281–289.

Carter Stewart R. et al. (2014). "Neutrophil Accumulation in the Small Intestine Contributes to Local Tissue Destruction Following Combined Radiation and Burn Injury". *Journal of Burn Care & Research* 37.2, pp. 97–105.

Chang JX et al. (2005). "Functional and morphological changes of the gut barrier during the restitution process after hemorrhagic shock". *World journal of gastroenterology* 11.35, p. 5485.

Chen MM et al. (2013). "Intoxication by Intraperitoneal Injection or Oral Gavage Equally Potentiates Postburn Organ Damage and Inflammation". *Mediators of Inflammation* 2013, pp. 1–10.

Crenn P et al. (2000). "Postabsorptive plasma citrulline concentration is a marker of absorptive enterocyte mass and intestinal failure in humans". *Gastroenterology* 119.6, pp. 1496–1505.

Curtis SB (1986). "Lethal and potentially lethal lesions induced by radiation–a unified repair model". *Radiation Research* 106.2, pp. 252–270.

Dant JT (2016). Estimating the Midline Tissue Dose in Murine Mammals from Photons. ARA/HS-TN-16-008-B, Arlington, VA: Applied Research Associates.

Ferguson A et al. (1977). "Technique for microdissection and measurement in biopsies of human small intestine". *Journal of Clinical Pathology* 30.11, pp. 1068–1073.

Galjaard H and D Bootsma (1969). "The regulation of cell proliferation and differentiation in intestinal epithelium. II. A quantitative histochemical and autoradiographic study after low doses of x-irradiation". *Experimental Cell Research* 58.1, pp. 79–92.

Galjaard H, W van der Meer-Fieggen, and J Giesen (1972). "Feedback control by functional villus cells on cell proliferation and maturation in intestinal epithelium". *Experimental Cell Research* 73.1, pp. 197–207.

Gozenbuk V and I Keirim-Markus (1988). *Dosimetric Criteria of the Severity of Acute ManIrradiation*. Moscow: Energoatomizdat.

Hamby DM (1994). "A review of techniques for parameter sensitivity analysis of environmental models". *Environmental monitoring and assessment* 32.2, pp. 135–154.

Hasan M and A Ferguson (1981). "Measurements of intestinal villi non-specific and ulcer-associated duodenitis-correlation between area of microdissected villus and villus epithelial cell count". *Journal of Clinical Pathology* 34.10, pp. 1181–1186.

Jeschke MG et al. (2007). "Gut Mucosal Homeostasis and Cellular Mediators after Severe Thermal Trauma and the Effect of Insulin-Like Growth Factor-I in Combination with Insulin-Like Growth Factor Binding Protein-3". *Endocrinology* 148.1, pp. 354–362.

Joiner M (2009). *Basic Clinical Radiobiology*. Ed. by Michael Joiner and Albert van der Kogel. Fourth Edition.

Kononenko AM and GV Farafonov (1969). "[Changes in the number of epithelial cells on small intestinal villi in irradiated mice]". *Radiobiologiia* 9.2, pp. 209–212.

Lea D (1955). *Action of Radiation on Living Cells, 2nd ed*. Cambridge: Syndics of the Cambridge University Press.

Lesher J and S Lesher (1970). "Effects of Single-Dose, Whole-Body, 60 Co Gamma Irradiation on Number of Cells in DNA Synthesis and Mitosis in the Mouse Duodenal Epithelium". *Radiation Research* 43.2, p. 429.

Lesher S (1967). "Compensatory Reactions in Intestinal Crypt Cells after 300 Roentgens of Cobalt-60 Gamma Irradiation". *Radiation Research* 32.3, p. 510.

MacVittie Thomas J. et al. (2012a). "The Prolonged Gastrointestinal Syndrome in Rhesus Macaques: The Relationship Between Gastrointestinal, Hematopoietic, and Delayed Multi-organ Sequelae Following Acute, Potentially Lethal, Partial-body Irradiation". *Health Physics* 103.4, pp. 427–453.

MacVittie TJ et al. (2012b). "The Acute Gastrointestinal Subsyndrome of the Acute Radiation Syndrome: A Rhesus Macaque Model". *Health Physics* 103.4, pp. 411–426.

Matsuzawa H et al. (1973). "Acute mortality and changes in body-weight of mice after partial-body irradiation with X-rays and fast neutrons". *International Journal of Radiation Biology and Related Studies in Physics, Chemistry, and Medicine* 24.3, pp. 275–283.

Matsuzawa T and R Wilson (1965). "The intestinal mucosa of germfree mice after whole-body X-irradiation with 3 kiloroentgens". *Radiation research* 25.1, pp. 15–24.

Meineke FA, CS Potten, and M Loeffler (2001). "Cell migration and organization in the intestinal crypt using a lattice-free model". *Cell Proliferation* 34.4, pp. 253–266.

Meysman F, T Petzoldt, and K Soetaert (2008). FME- Flexible Modelling Environment: sensitivity analysis, parameter identifiability, parameter estimation of models consisting of differential equations.

Nesterenko VS and AV Piskarev (1983). "Changes in small intestine function after radiation and thermal injury". *Radiobiologiia* 23.3, pp. 404–406.

Patel DD et al. (2012). "Radioprotection to small intestine of the mice against ionizing radiation by semiquinone glucoside derivative (SQGD) isolated from Bacillus sp. INM-1". *Molecular and Cellular Biochemistry* 370.1-2, pp. 115–125.

Potten Christopher S. and H. K. Grant (1998). "The relationship between ionizing radiation-induced apoptosis and stem cells in the small and large intestine." *British journal of cancer* 78.8, p. 993.

Potten Christopher S. and Markus Loeffler (1990). "Stem cells: attributes, cycles, spirals, pitfalls and uncertainties. Lessons for and from the crypt". *Development* 110.4, pp. 1001–1020.

Quastler H (1956). "The Nature of Intestinal Radiation Death". *Radiation Research* 4.4, p. 303.

Quastler H and FG Sherman (1959). "Cell population kinetics in the intestinal epithelium of the mouse". *Experimental cell research* 17.3, pp. 420–438.

R Core Team (2013). R: A Language and Environment for Statistical Computing. R Foundation for Statistical Computing. Vienna, Austria.

Ramzy PI et al. (2000). "Gut epithelial apoptosis after severe burn: effects of gut hypoperfusion". *Journal of the American College of Surgeons* 190.3, pp. 281–287.

Rijke R (1977). "Control mechanisms of cell proliferation in intestinal epithelium". PhD thesis. Erasmus MC: University Medical Center Rotterdam.

Rijke RP et al. (1976). "The effect of ischemic villus cell damage on crypt cell proliferation in the small intestine: evidence for a feedback control mechanism". *Gastroenterology* 71.5, pp. 786–792.

Sato F et al. (1972). "Radiation effects on cell populations in the intestinal epithelium of mice and its theory". *Cell and Tissue Kinetics* 5.3, pp. 227–235.

Savidge TC, JA Walker-Smith, and AD Phillips (1995). "Novel insights into human intestinal epithelial cell proliferation in health and disease using confocal microscopy." *Gut* 36.3, pp. 369–374.

Schultze B et al. (1972). "Autoradiographic Investigation on the Cell Kinetics of Crypt Epitherlia in the Jejunum of the Mouse Confirmation of Steady State Growth with Constant Frequency Distribution of Cells Throughout the Cell Cycle". *Cell Proliferation* 5.2, pp. 131–145.

Sherman FG and H Quastler (1960). "DNA synthesis in irradiated intestinal epithelium". *Experimental Cell Research* 19, pp. 343–360.

Smirnova OA (2010). *Environmental Radiation Effects on Mammals*. Springer.

Smit JM et al. (1986). "Gastrointestinal toxicity of chemotherapy and the influence of hyperalimentation". *Cancer* 58.9, pp. 1990–1994.

Soetaert K, T Petzoldt, and W Setzer (2015). deSolve: Differential Equations in R.

Trier JS and TH Browning (1966). "Morphologic response of the mucosa of human small intestine to x-ray exposure". *The Journal of Clinical Investigation* 45.2, pp. 194–204.

Tyazelova V (1988). *Dynamics of Haemopoiesis*. Moscow: Meditsina.

Wang J et al. (2015). "Total Body Irradiation in the "Hematopoietic" Dose Range Induces Substantial Intestinal Injury in Non-Human Primates". *Radiation Research* 184.5, pp. 545–553.

Wentz J. (2015). Parameterization of Small Intestine Model of Radiation Injury in Mice and Humans. ARA/HS-TN-15-006-A, Arlington, VA: Applied Research Associates.

Wolf SE et al. (1999). "Cutaneous burn increases apoptosis in the gut epithelium of mice". *Journal of the American College of Surgeons* 188.1, pp. 10–16.

Wright N et al. (1973). "The cell cycle time in the flat (avillous) mucosa of the human small intestine". *Gut* 14.8, pp. 603–606.

Wright NA and A Al-Nafussi (1982). "The kinetics of villus cell populations in the mouse small intestine. II. Studies on growth control after death of proliferative cells induced by cytosine arabinoside, with special reference to negative feedback mechanisms". *Cell and Tissue Kinetics* 15.6, pp. 611–621.

Wright NA and M Irwin (1982). "The kinetics of villus cell populations in the mouse small intestine". *Cell Proliferation* 15.6, pp. 595–609.

7 Abbreviations, Acronyms and Symbols

ARA	Applied Research Associates, Inc.
ARS	Acute radiation syndrome
d	Days
DE	Differential Evolution
DTRA	Defense Threat Reduction Agency
FIA	Free-in-Air
FME	Flexible Modeling Environment
GIM	Gut Injury Model
Gy	Gray
HENRE	Health Effects from Nuclear and Radiological Environments
LPL	Lethal and Potentially Lethal
MLT	Midline tissue
na	Not available
NHP	Non-human primate
ODE	Ordinary differential equation
PAIR	Proliferation and Intracellular Repair
RIPD	Radiation-Induced Performance Decrement
R	Roentgen
WMD	Weapon of Mass Destruction
% TBSA	Percent of total body surface area

A Mathematical Model of the Small Intestine Cell Kinetics

This section provides a comprehensive list of parameters, variables and equations describing the small intestine cell kinetic model. Table A.1 lists each parameter and variable of the model with their biological description.

Table A.1: Biological descriptions, parameters and variables in the small intestine mathematical model.

Component	Biological Description	Units
$x = x^{ud} + x^{d}$	Number of proliferating crypt cells	cells/column
x^{ud}	Number of undamaged proliferating crypt cells	cells/column
x^{d}	Number of damaged proliferating crypt cells	cells/column
y	Number of maturing crypt cells	cells/column
z	Number of villus cells	cells/column
B	Rate of proliferation	d^{-1}
γ	Transit rate through proliferative compartment	d^{-1}
F	Transit rate through maturation compartment	d^{-1}
E	Transit rate through villus compartment	d^{-1}
G	Constant upregulation of mediator	(cells/column)d^{-1}
H	Rate of downregulation of mediator by epithelial cells	(cells/column)$^{-1}\mathrm{d}^{-1}$
K	Mediator feedback threshold	cells/column
α	Maximum rate of proliferative compartment repopulation	d^{-1}
δ	Minimum maturation rate through maturation compartment	d^{-1}
ψ	Minimum transit rate through villus compartment	d^{-1}
θ	Relative effect of maturing crypt cells on repopulation rate	-
ϑ	Relative effect of villus cells on repopulation rate	-
$L = l/\gamma$	Effect of proliferation on transit rate through maturation compartment	d
$M = m/\gamma$	Effect of proliferation on transit rate through villus compartment	d
D_0	Specifies radiosensitivity of X cells	Gy
n	Number of targets, X cells	-
ν	Rate of damaged cell death	d^{-1}
ϕ	Relative effect of damaged cells on repopulation rate	-
S	Burn size	%TBSA
a_0	Determines duration of burn effect on villus death	d^{-1}
b_0	Describes maximum effect on villus death	-
a_1	Determines duration of burn effect on proliferation	d^{-1}
b_1	Describes maximum effect of burn on proliferation	-
k	Activation threshold for burn effect	%TBSA
Δ_b	Delay after burn before proliferation suppression	d

Equations A.1 - A.8 define the normalized small intestine cell kinetic model, where we denote the normalized undamaged proliferating cells, damaged proliferating cells, maturing crypt cells and villus cells as $\widetilde{x}^{ud}$, $\widetilde{x}^{d}$, $\widetilde{y}$ and $\widetilde{z}$, respectively. Using the initial conditions in Equations A.9 and A.10, the model simulates an acute combined radiation dose of D Gy (MLT) and thermal injury (S% TBSA) applied at time $t = 0$ d.

$$\dot{\widetilde{x}}^{ud} = \gamma\widetilde{x}^{ud}(\widetilde{B} - 1) - W_1(S,t)\widetilde{x}^{ud} \tag{A.1}$$

$$\dot{\widetilde{x}}^{d} = -\nu\dot{\widetilde{x}}^{d} \tag{A.2}$$

$$\dot{\widetilde{y}} = \delta\left((1+l)\widetilde{x}^{ud} - (1+l\widetilde{B})\widetilde{y}\right) \tag{A.3}$$

$$\dot{\widetilde{z}} = \psi\left(\frac{1+m}{1+l}(1+l\widetilde{B})\widetilde{y} - (1+m\widetilde{B})\widetilde{z}\right) - W_0(S,t)\widetilde{z} \tag{A.4}$$

$$\widetilde{B} = \frac{\alpha/\gamma}{1 + b(\widetilde{x}^{ud} + \phi\widetilde{x}^{d} + \theta\widetilde{y}\frac{\gamma}{\delta(1+l))} + \vartheta\widetilde{z}\frac{\gamma}{\psi(1+m)})} \tag{A.5}$$

$$b = \frac{\alpha/\gamma - 1}{1 + \frac{\theta\gamma}{\delta(1+l)} + \frac{\vartheta\gamma}{\psi(1+m)}} \tag{A.6}$$

$$W_0(S,t) = b_0\frac{S}{S+k}e^{-a_0 t} \tag{A.7}$$

$$W_1(S,t) = \begin{cases} b_1\frac{S}{S+k}e^{-a_1 t(100-S)} & t > \Delta_b \\ 0 & t \leq \Delta_b \end{cases} \tag{A.8}$$

$$\widetilde{x}^{ud}(0) = 1 - (1 - e^{-D/D^0})^n \tag{A.9}$$

$$\widetilde{x}^{d}(0) = (1 - e^{-D/D^0})^n \tag{A.10}$$

The parameters in Table A.2 can be used to simulate small intestine cell kinetics of either humans or mice.

Table A.2: Murine and human parameters.

Parameter	Murine Value	Human Value
γ	1.446 d^{-1}	0.18 d^{-1}
α	2.87 d^{-1}	2.589 d^{-1}
l	2.456	1.64
δ	0.341 d^{-1}	0.305 d^{-1}
m	1.639	1.889
ψ	0.284 d^{-1}	0.064 d^{-1}
θ	942.632	11.899
ϑ	35.633	4.633
D_0	6.054 Gy	6.005 Gy
n	1	2
ν	1.011 d^{-1}	2.727 d^{-1}
ϕ	108.193	743.469
a_0	54.919 d^{-1}	1.458 d^{-1}
b_0	47.986	1.346
a_1	0.001 d^{-1}	0.001 d^{-1}
b_1	0.767	0.123
k	0.008% TBSA	1% TBSA
Δ_b	1 d	1 d

B Supplementary Figures

This section provides figures supplemental to the report. Figure B.1 presents simulations of epithelial recovery experiments of rodents from insults other than radiation or burn. Figures B.2-B.12 present simulations of rodent acute radiation experiments. All of the data in this section were used to optimize parameters of the murine model. In each figure, simulation results (solid red lines) are compared to experimental data (black triangles), and error bars represent ± standard deviations.

B.1 Additional Rodent Insult Experiments

We examined the ability of the model to simulate crypt and villus data from experiments in Rijke et al., 1976 and Wright and Al-Nafussi, 1982. In Rijke et al., 1976, villus clamping killed villus cells in the small intestine of a rat, and crypt and villus cells were measured 2, 8, 16 and 24 hours post-clamping. In Wright and Al-Nafussi, 1982, cytosine arabinoside killed off most proliferating crypt cells before the epithelial cells were allowed to return to their original values. During the return to homeostasis, crypt and villus cells were measured once daily for 18 days following the cytosine arabinoside injections. Figure B.1 shows the model simulations of these experiments with the murine small intestine model. Although the model initially captures the dynamics of crypt and villus cells in response to cytosine arabinoside, the amplitude of the second rebound (negative for villus cells, positive for crypt cells) is not reproduced.

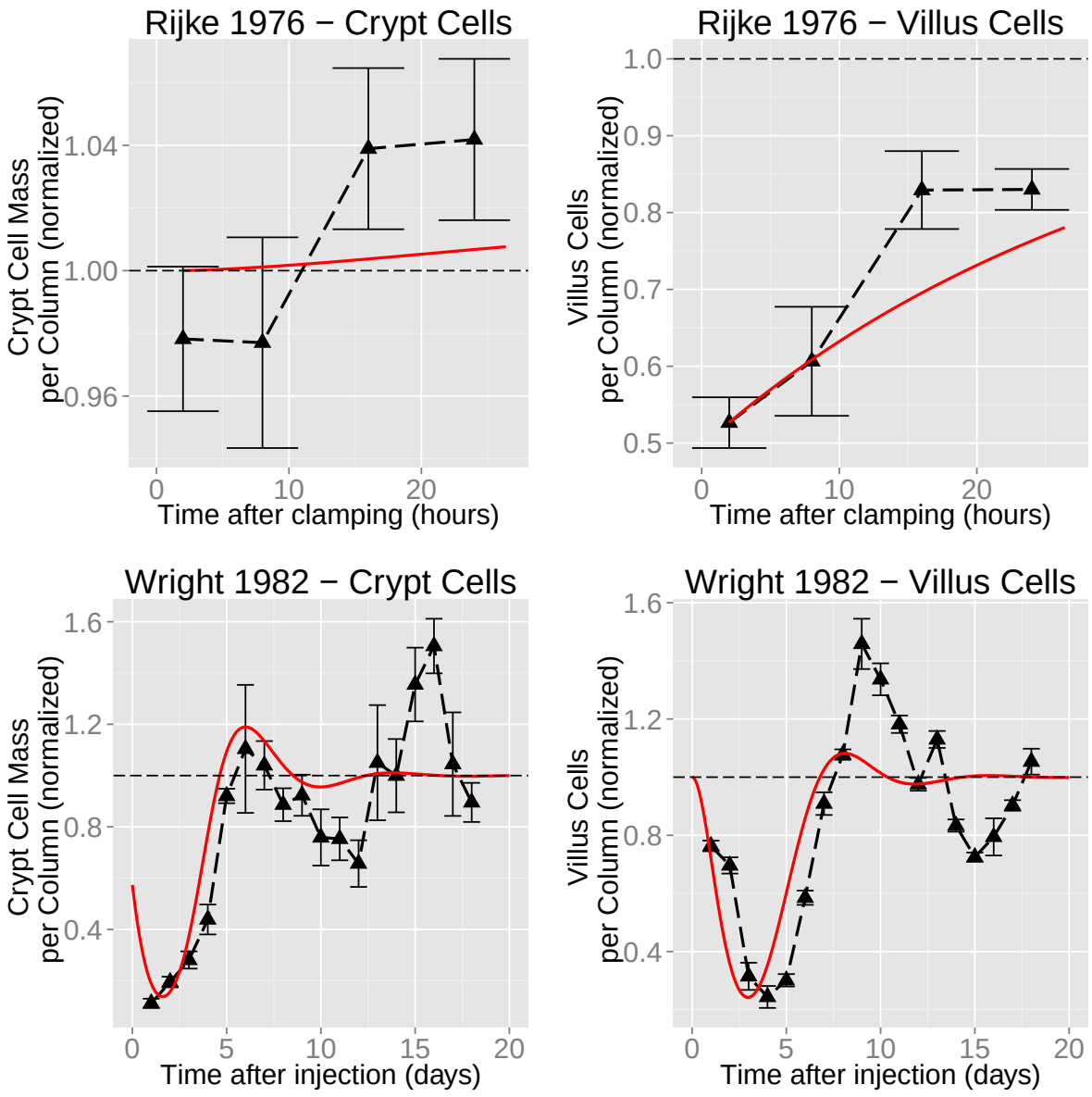

Figure B.1: Simulations of non-radiation rodent insult experiments.

B.2 Rodent Radiation Experiments

The following section provides simulations of the murine model against mice and rat acute radiation experimental data. This data was used with the data in Section B.1 to optimize all parameters (not related to burn) of the murine model. The complete list of rodent radiation data can be found in Table 3.5.

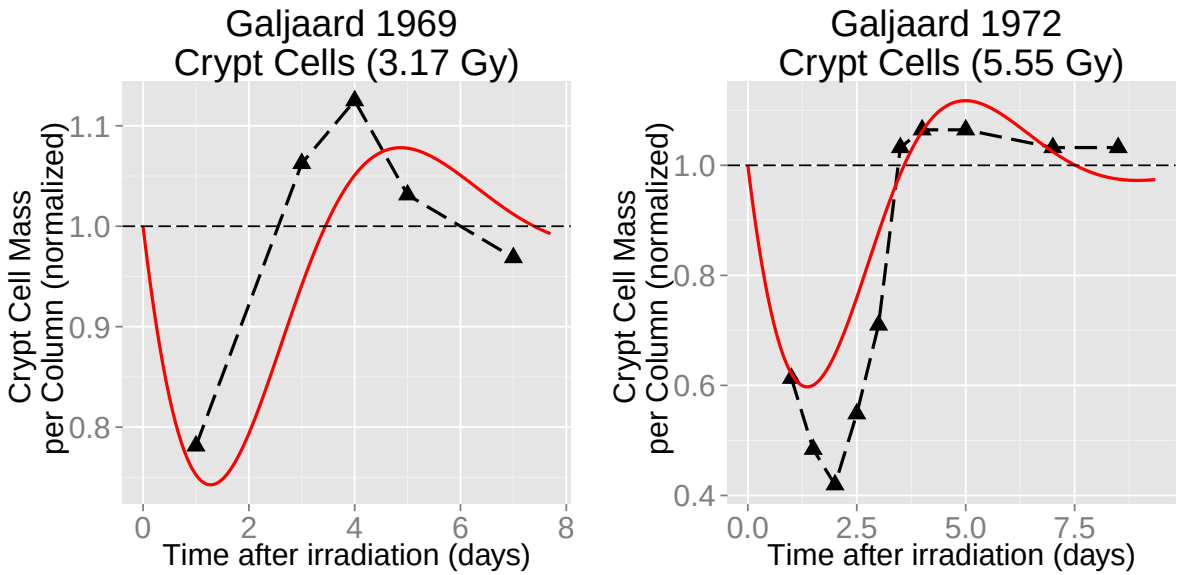

Figure B.2: Simulations of the Galjaard and Bootsma, 1969 and Galjaard et al., 1972 experiments.

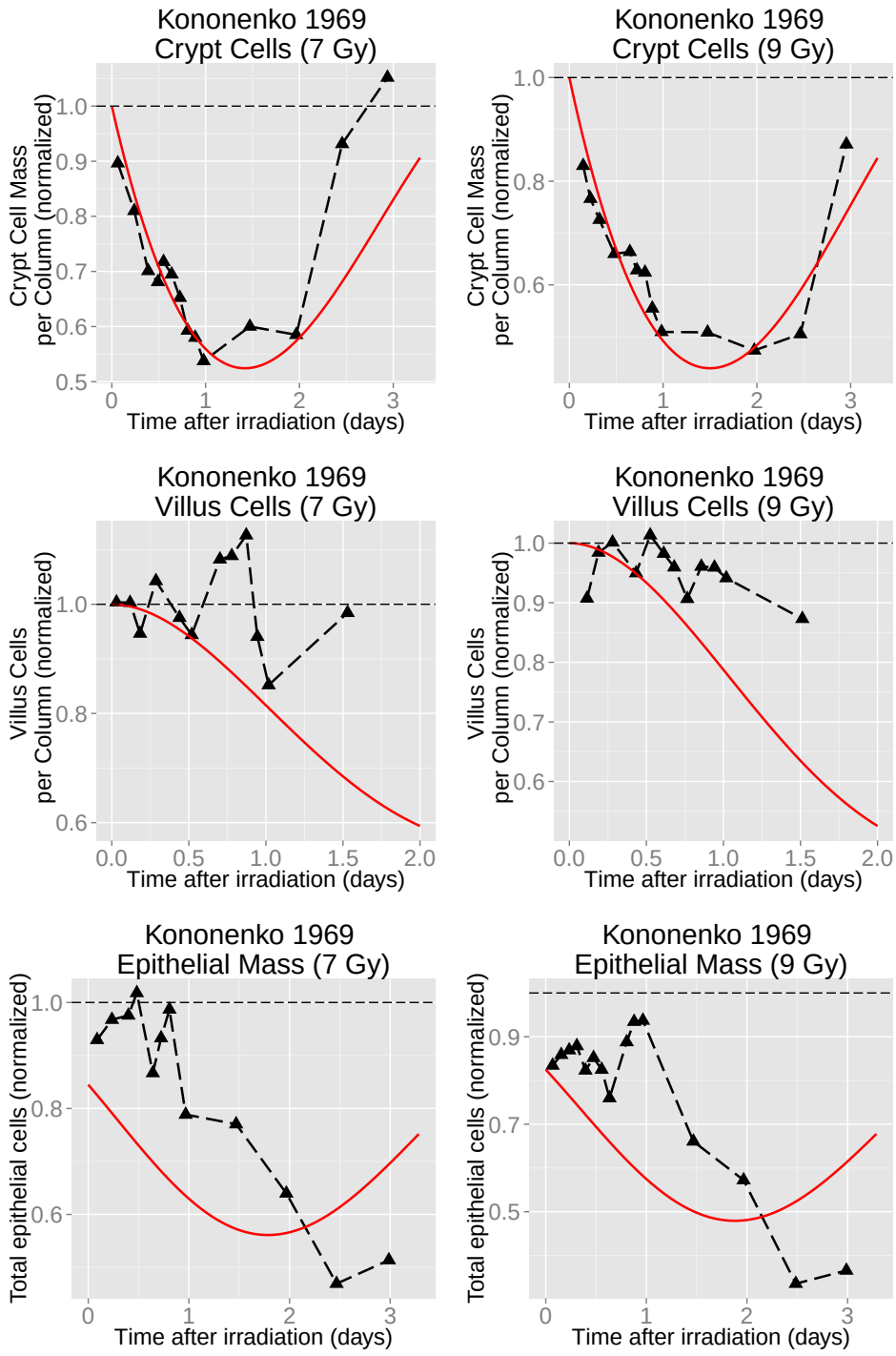

Figure B.3: Simulations of the Kononenko and Farafonov, 1969 experiments.

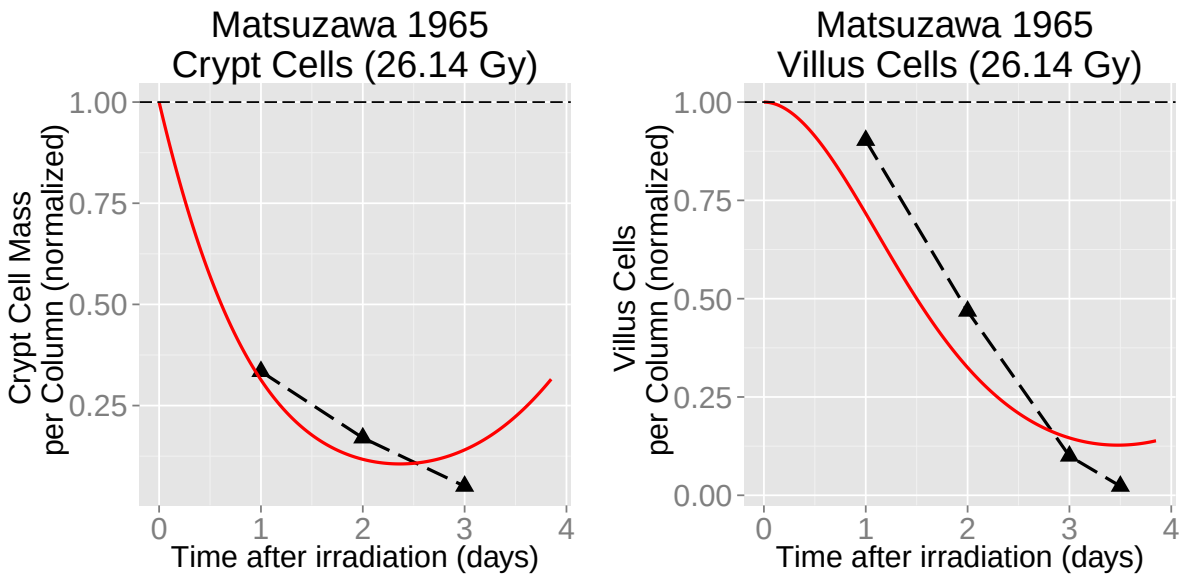

Figure B.4: Simulations of the Matsuzawa and Wilson, 1965 experiments.

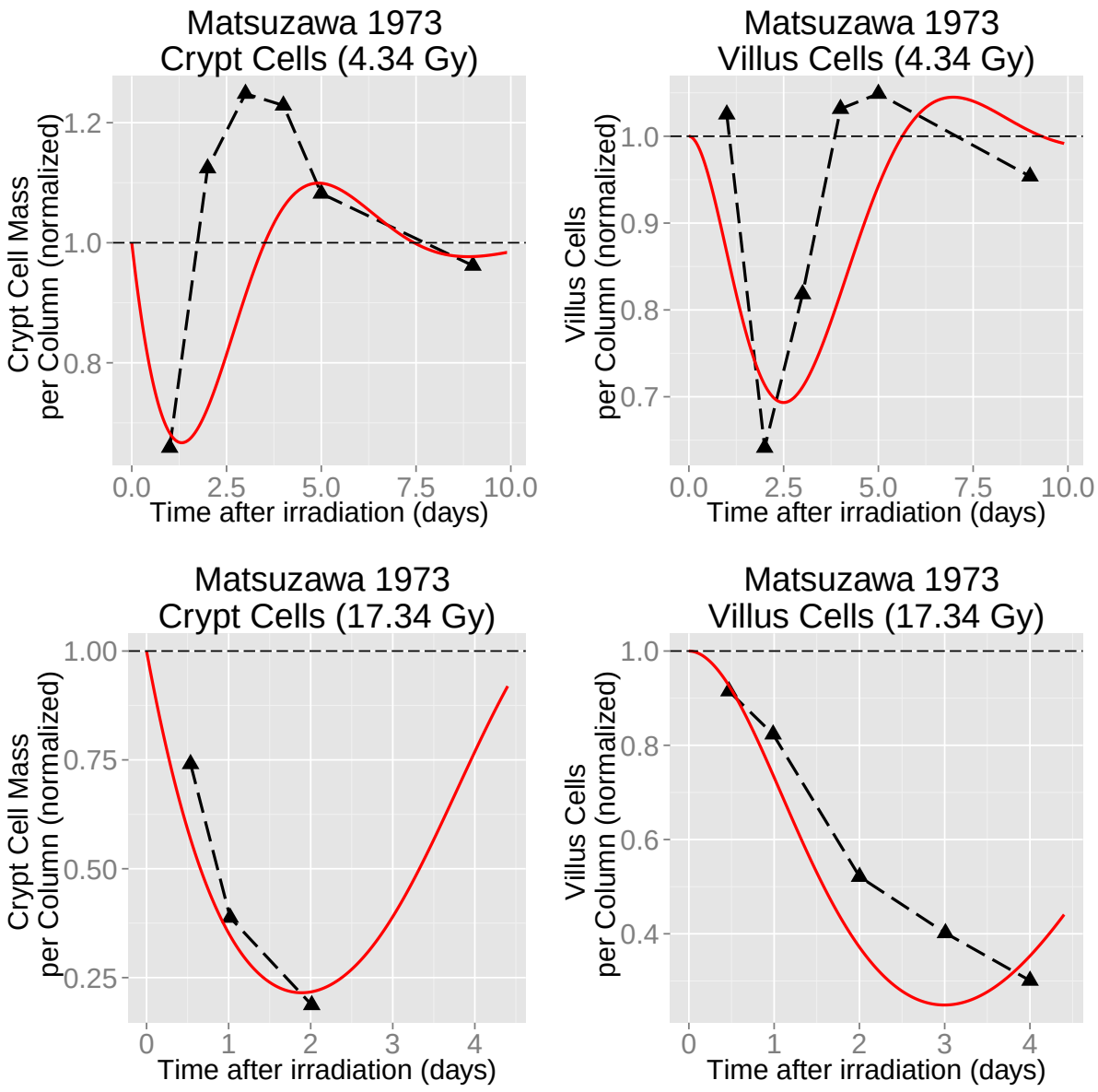

Figure B.5: Simulations of the Matsuzawa et al., 1973 experiments.

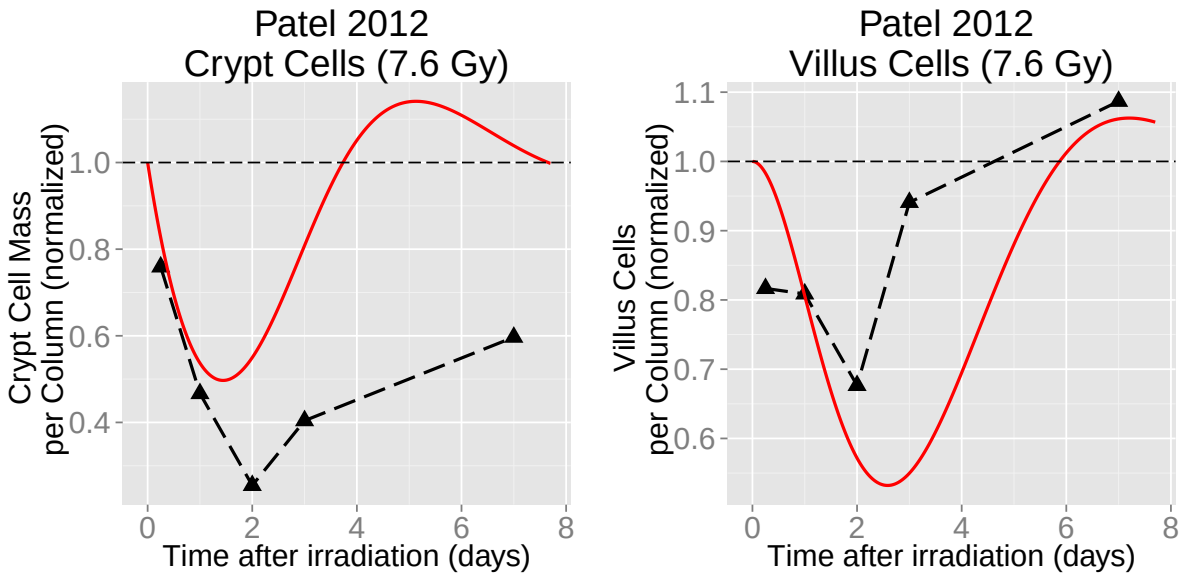

Figure B.6: Simulations of the Patel et al., 2012 experiments.

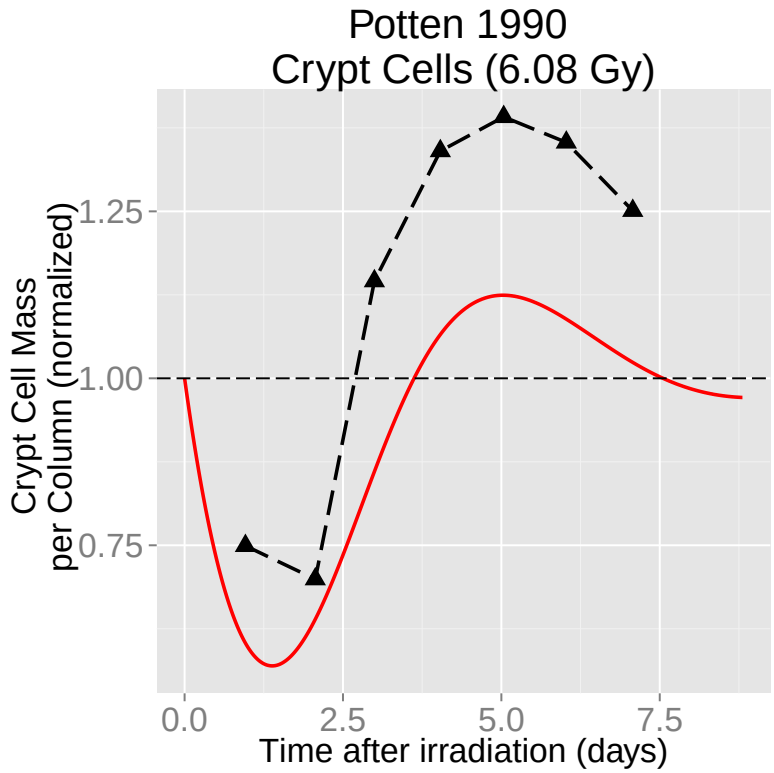

Figure B.7: Simulations of the Potten and Loeffler, 1990 experiments.

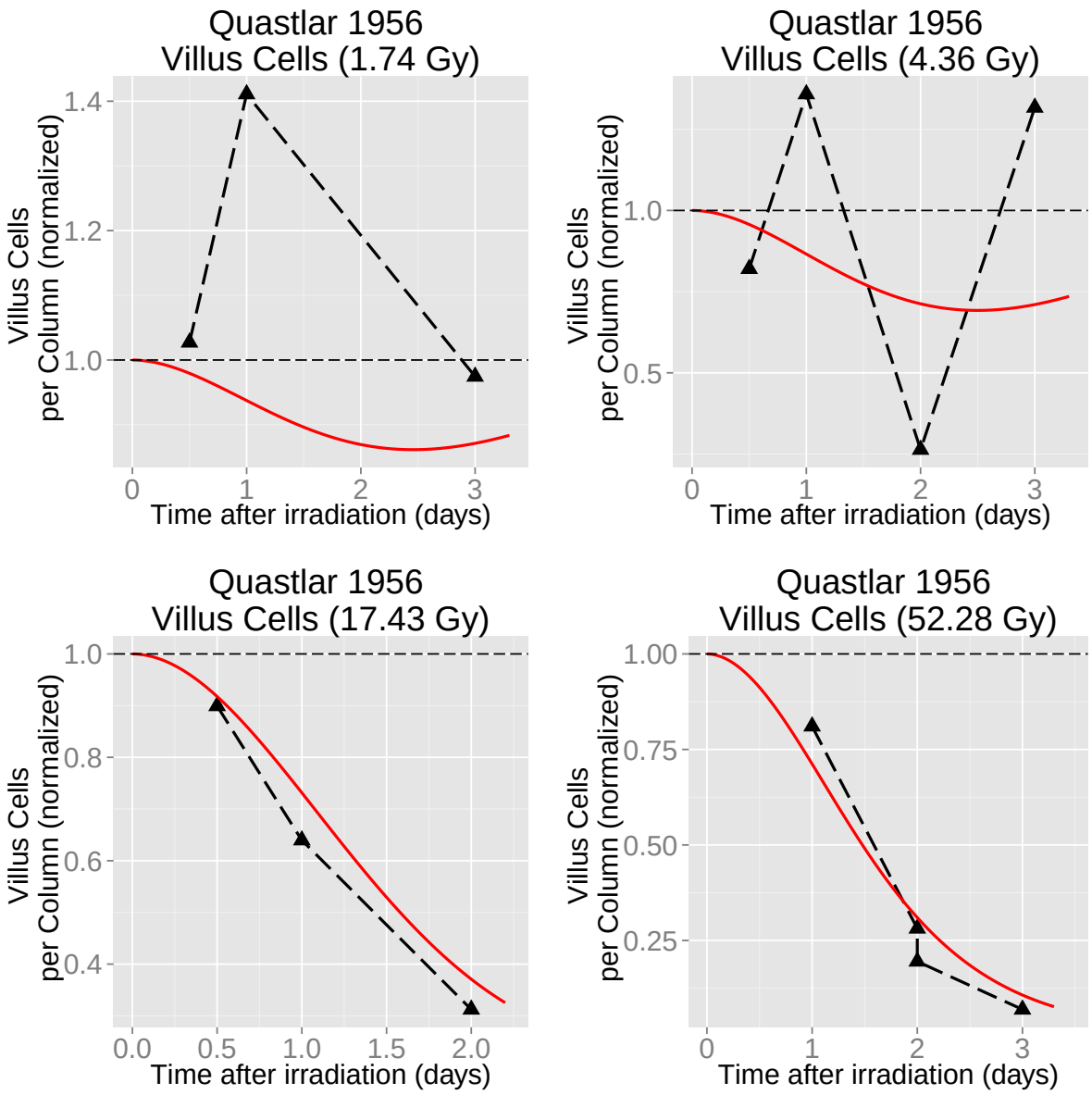

Figure B.8: Simulations of the Quastler, 1956 experiments.

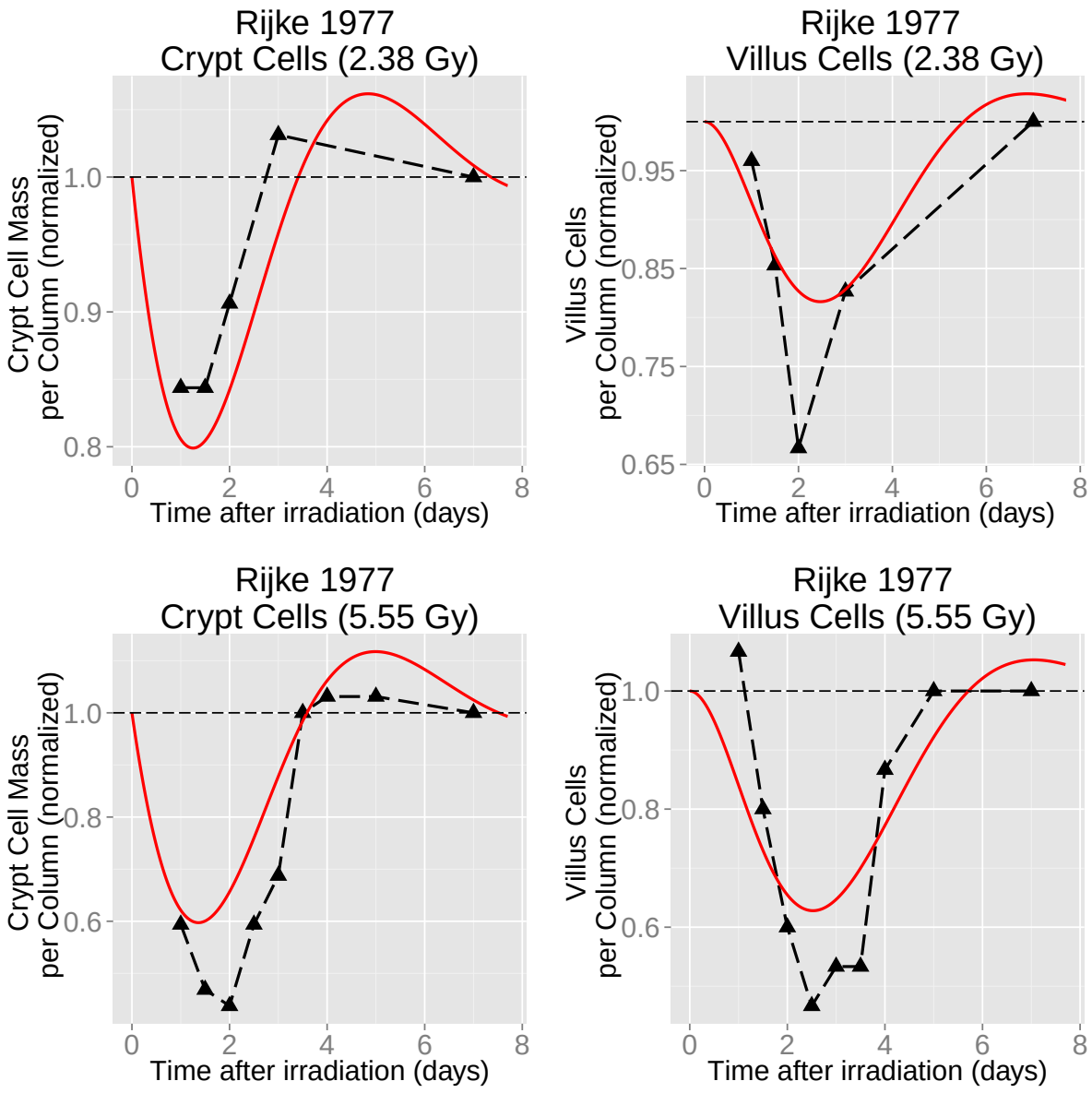

Figure B.9: Simulations of the Rijke, 1977 experiments.

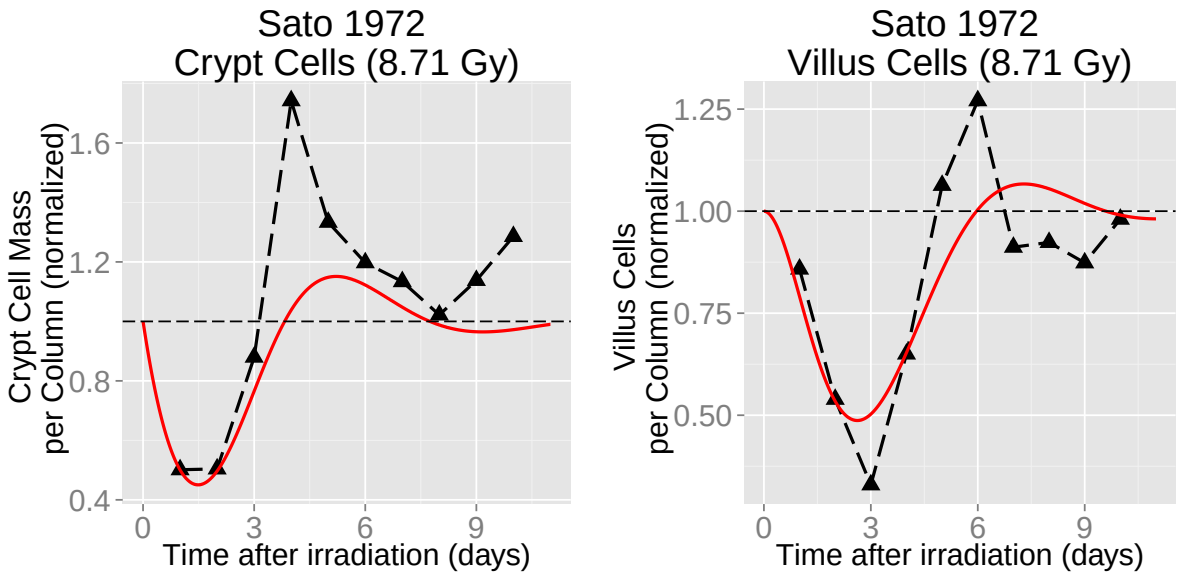

Figure B.10: Simulations of the Sato et al., 1972 experiments.

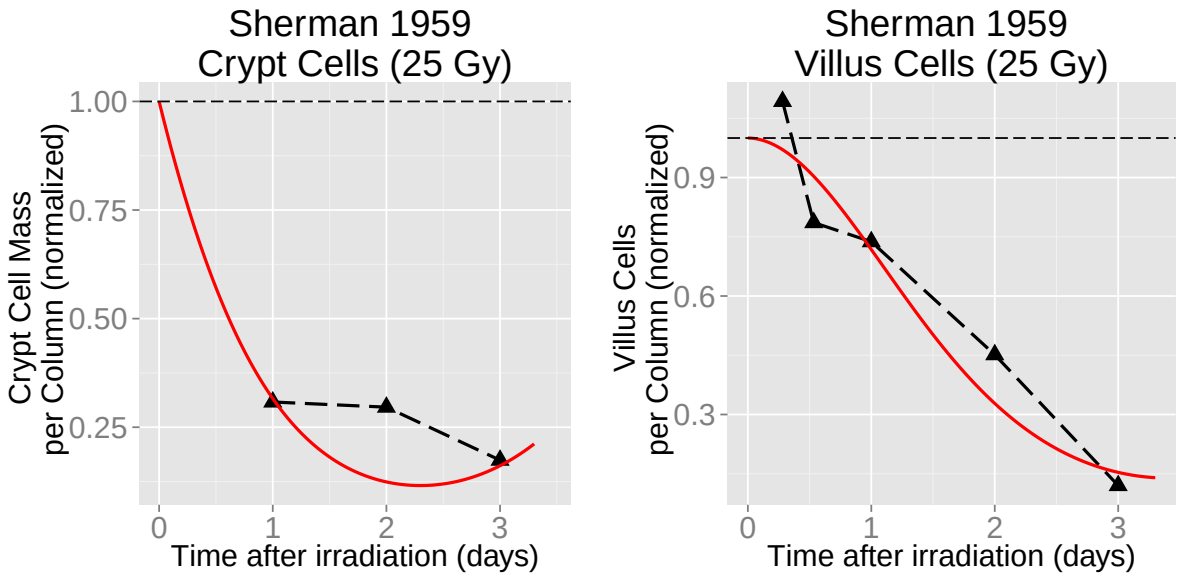

Figure B.11: Simulations of the Sherman and Quastler, 1960 experiment.

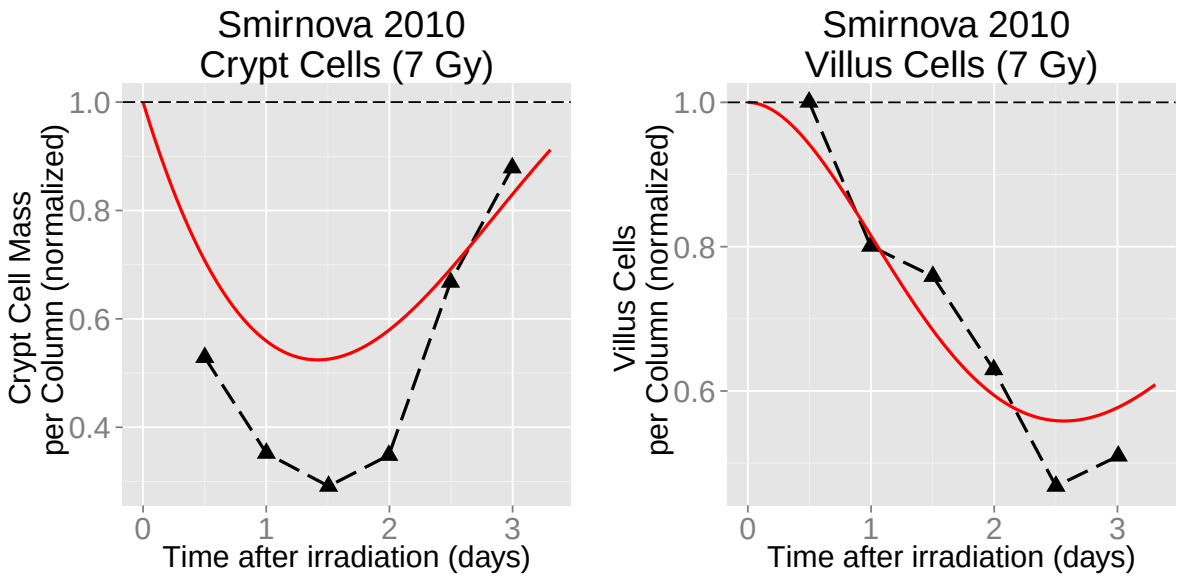

Figure B.12: Simulations of an experiment reported in Smirnova, 2010.

B.3 Villus Height and Cell Count

According to rat data from Rijke, 1977, normalized villus height is approximately equal to normalized villus cell counts. This is reasonable, as the circumference of each villus remains relatively constant as the length increases. To demonstrate this, we present data from Rijke, 1977 in Figure B.13 (red triangles), which reported villus lengths and villus cell counts after various radiation doses. The best-fit line for this data including the origin (black dashed line) is close to the identity ($y = 0.016 + 0.94 \cdot x$) and fits the data very well ($r^2 = 0.993$). From this, we assume normalized villus height is a reasonable approximation of normalized villus cell counts.

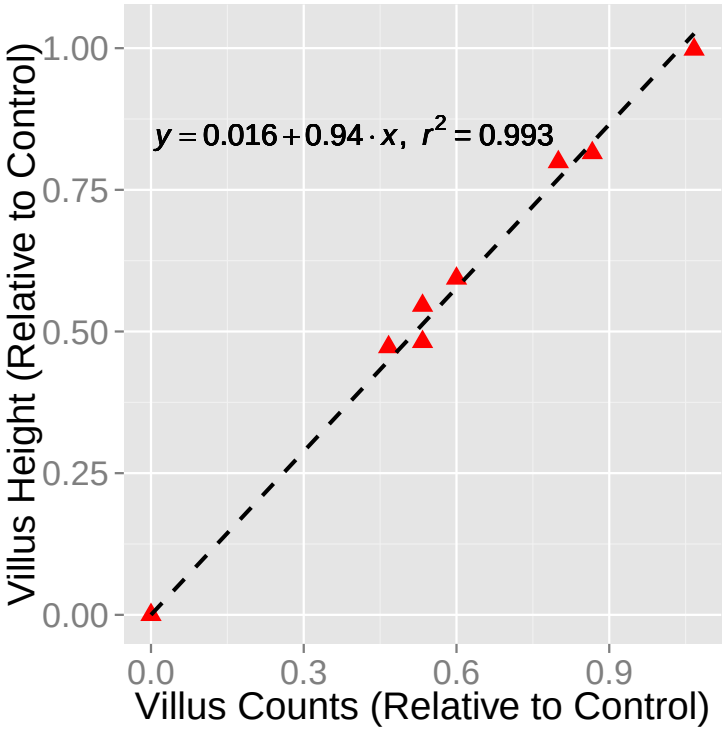

Figure B.13: Plot of villus height against villus counts measured in Rijke, 1977.

C Human Extrapolation

We do not have the human data required to quantify the components of burn response, which makes it very difficult to extrapolate parameters for a human model. To circumnavigate this problem, we extrapolate parameters from murine kinetics. For our approach, we compare human and murine responses to radiation in order to make assumptions about murine and human differences in burn response.

Two key components of response to insult are timing and amplitude. We fit the human model to villus cell data which has been scaled (in time and amplitude) from murine burn data. We set the scaling factors based on the timing and amplitude of human and murine responses to radiation. In particular, we compared the villus cell count nadirs following an acute radiation dose of 5 Gy. With these relationships, we extrapolated synthetic human burn data from the data used to optimize the murine burn parameters (Table 3.7).

In this section, we differentiate between murine and human parameters with m and h subscripts, respectively (the human parameter a_0 becomes $a_{0,h}$, for example). For simplicity, we assume the delay time of proliferation suppression is equal for murine and human models ($\Delta_{b,h} = \Delta_{b,m} = 1$). We found the normalized villus cell nadirs of the murine model $(t_{n5,m}, z_{n5,m})$ and the human model $(t_{n5,h}, z_{n5,h})$, and used these values to scale the time and values of normalized murine villus cell burn data (t_i, v_i) to produce synthetic human data:

$$(\frac{t_{n5,h}}{t_{n5,m}} t_i, \frac{v_{n5,h}}{v_{n5,m}} v_i). \tag{C.1}$$

We fit the human burn parameters to the synthetic data (Eq.C.1), adopting the same approach used to parameterize the murine burn response. The parameter values resulting from this approach are provided in Table C.1 and simulations of moderate radiation (5 Gy) and burn (15% TBSA) insults with these parameter values are presented in Figures C.1 and C.2.

Table C.1: Extrapolated human burn parameters

Parameter	Human Value	Murine Value
a_0	54.919 d^{-1}	1.458 d^{-1}
b_0	47.986	1.346
a_1	0.001 d^{-1}	0.001 d^{-1}
b_1	0.767	0.123
k	0.008% TBSA	1% TBSA
Δ_b	1 d	1 d

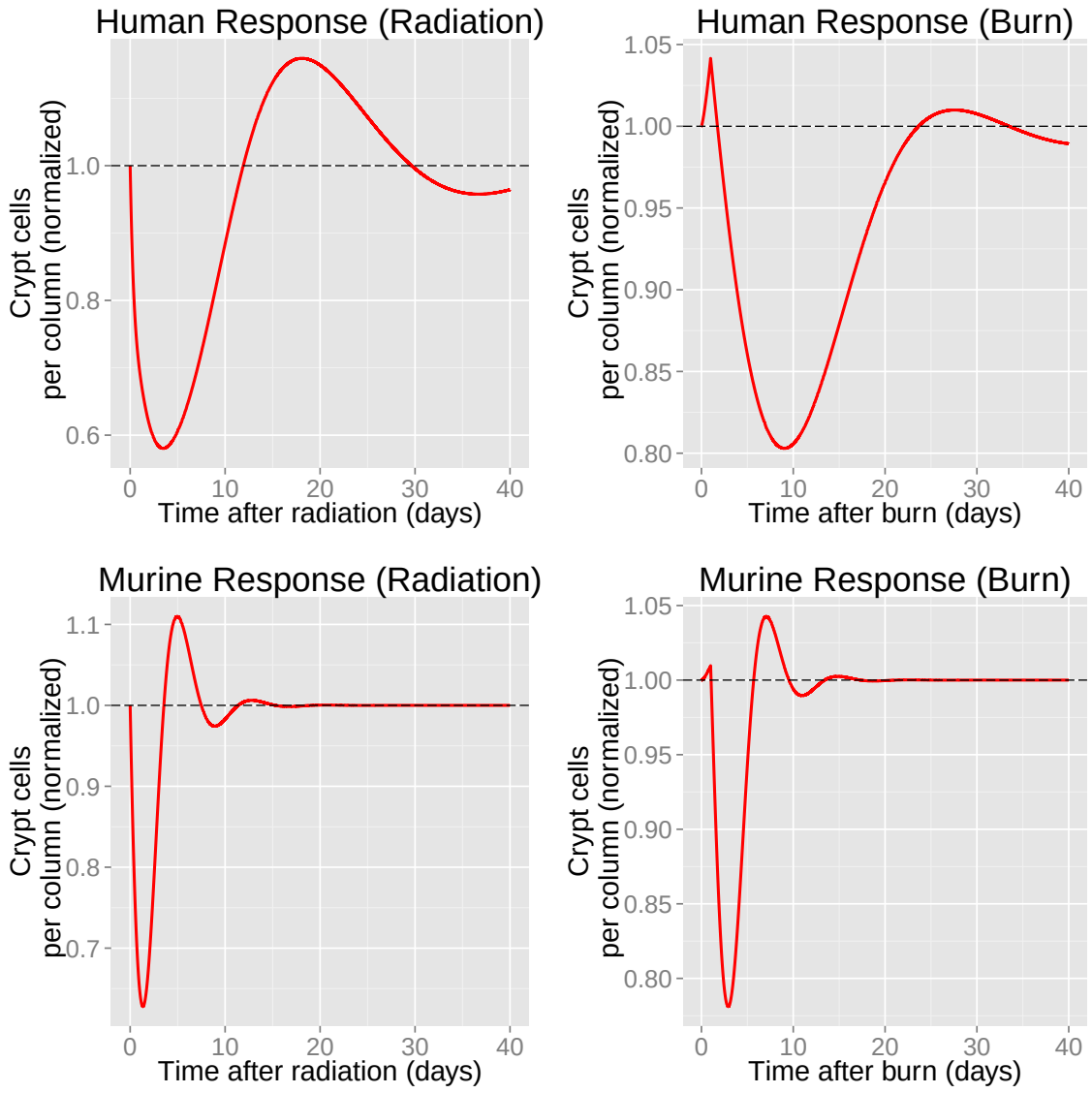

Figure C.1: Crypt cell simulations for human and murine models responding to radiation and burn.

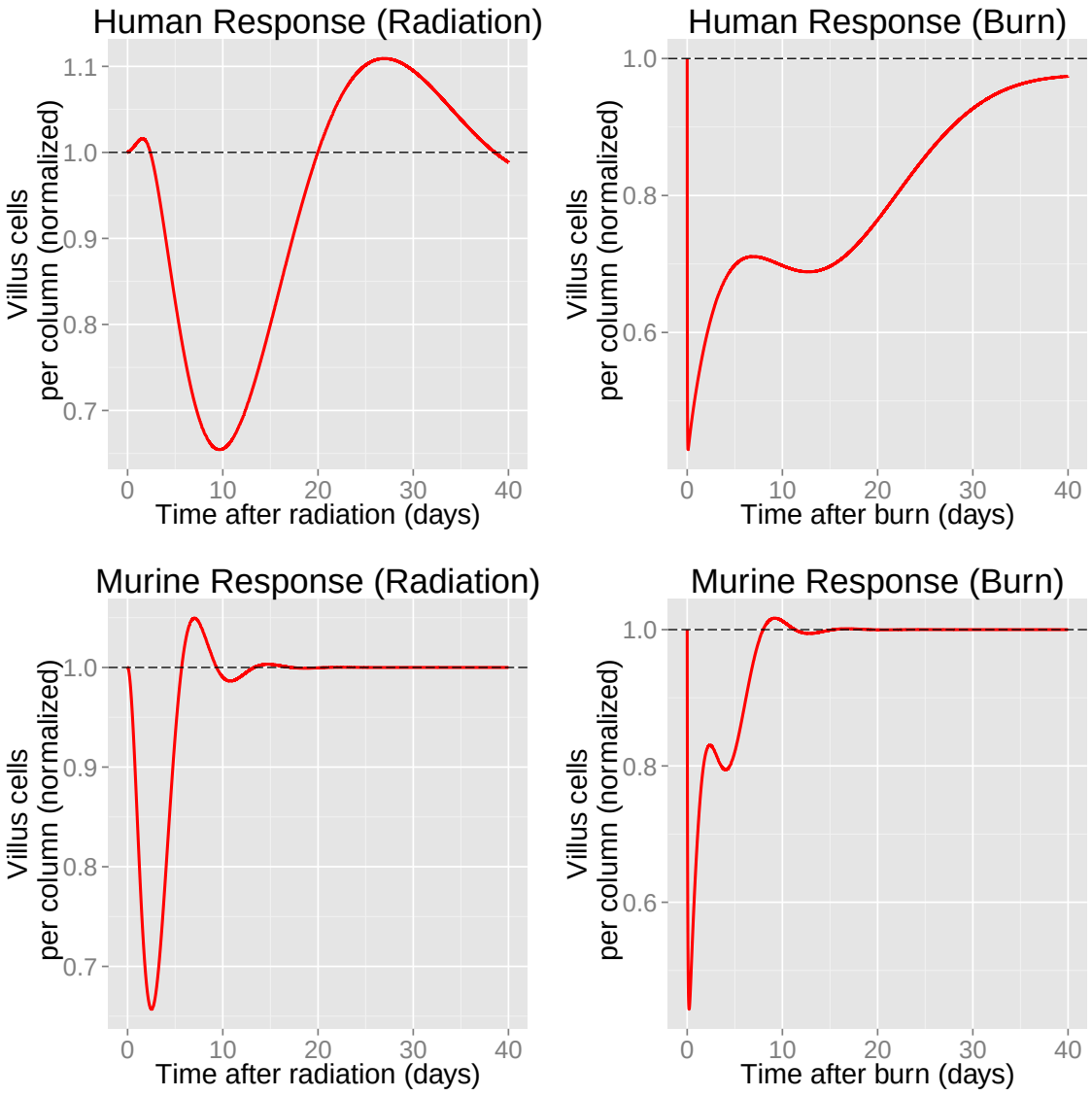

Figure C.2: Villus cell simulations for human and murine models responding to radiation and burn.